Aalto University Publications in Materials Science and Engineering
Aalto-yliopiston materiaalitekniikan julkaisuja
Espoo 2010 TKK-MT-216

Thermodynamics and Phase Equilibria in the (Ni, Cu, Zn)-(As, Sb, Bi)-S Systems at Elevated Temperatures (300 – 900^{o}C)

F. Tesfaye Firdu, P. Taskinen

Aalto-yliopisto Teknillinen korkeakoulu
Aalto-universitetet Tekniska högskolan
Aalto University School of Science and Technology

Aalto University Publications in Materials Science and Engineering
Aalto-yliopiston materiaalitekniikan julkaisuja
Espoo 2010 TKK-MT-216

Thermodynamics and Phase Equilibria in the (Ni, Cu, Zn)-(As, Sb, Bi)-S Systems at Elevated Temperatures (300 – 900^{o}C)

F. Tesfaye Firdu, P. Taskinen

Aalto University School of Science and Technology
Department of Materials Science and Engineering
Thermodynamics and Modeling of Metallurgical Processes (TDM)

Aalto-Yliopiston Teknillinen korkeakoulu
Materiaalitekniikan Laitos
Metallurgisten Prosessien Termodynamiikka ja Mallinnus (TDM)

Research program: ELEMET - Energy & Lifecycle Efficient Metal Processes
Project: ISS (Improved Sulfide Smelting)
Financers: Boliden Harjavalta Oy, Boliden Kokkola Oy, Norilsk Nickel Finland Oy, Outotec Oyj and the Finnish Funding Agency for Technology and Innovation (Tekes)
Keywords: Sulfides, Sulfosalt, Phase equilibrium, Thermodynamic property

Distribution:
Aalto University School of Science and Technology
Department of Materials Science and Engineering
P.O. Box 16200
FI-00076 Aalto, Finland
Tel. +358 9 470 22796
Fax. +358 9 470 22798
E-mail: Fiseha.Tesfaye@tkk.fi

ISBN 978-952-3273-3
ISSN 1455-2329

Multiprint Oy
Espoo 2010

Abstract

Stable phase relations in the (Ni, Cu)-(As, Sb)-S, Cu-Bi-S and Zn-As-S systems and their thermodynamic properties, at the presence of the impurities, are reviewed. The Cu-based systems are relatively intensively studied. Among the sulfosalts of these systems tetrahedrite ($Cu_{12+x}Sb_{4+y}S_{13}$, where $0 \leq x \leq 1.92$ and $-0.02 \leq y \leq 0.27$) and tennantite ($Cu_{12+x}As_{4+y}S_{13}$, where $0 < x < 1.72$ and $0 < y < 0.08$) are reported to be the most stable relative to other sulfosalts and certain other sulfide phases, which accounts for their common occurrence in a variety of mineral ore deposits. Natural tetrahedrite and tennantite in equilibrium with other minerals commonly constitute other chemical elements as a substitution for Cu, As and Sb and both are described by the general formula: $(Cu, Ag)_{10}(Fe, Zn, Cu, Hg, Cd, Co, Au)_2(Sb, As)_4S_{13}$. According to the literature data the Ni-based systems comprise a single stoichiometric ternary stable phase for their respective impurities (gersdorffite, NiAsS and ullmannite, NiSbS), and both experience a wide solid solubility range. At favorable conditions substitution of As for S in the gersdorffite and Co for Ni and Sb for As in the ullmennite are the main mechanisms of solid solution formations. Thermodynamic properties and phase equilibria studies in the Zn-As-S system are rare among published works. A study about this system, below 760^{o}C, has shown that there is no ternary phase stable.

In general, the ternary systems have complex phase-relations, which may be as a result of the very low differences in their Gibbs energies of formation.

Table of Contents

Symbols, Abbreviations, Units

B.P	boiling point [^oC]
X_i	composition of component i
L	liquid
T_{liq}	liquidus temperature [^oC]
T_m	melting temperature [^oC]
P	pressure [atm]
ss	solid solution
T_{sol}	solidus temperature [^oC]
ΔH^o	standard enthalpy [kJ/mol]
ΔS^o	standard entropy [kJ/mol·K]
ΔG^o	standard Gibbs energy [kJ/mole of a sulfosalt or sulfide]
ΔG_f	standard Gibbs energy of formation [kJ/mol of a sulfosalt or sulfide]
ΔG_r	standard Gibbs energy of reaction [kJ/mol of a sulfosalt or sulfide]
S.P	sublimation point [^oC]
T	temperature [^oC]

1 Introduction

Recently the availability of high grade Ni-, Cu- and Zn-sulfide ores is decreasing. Impurities such as As, Sb and Bi are commonly associated with the sulfide ores. The presence of these impurities affects the extractive metallurgy of the valuable metals. They cause the formation of undesired melts during roasting, the production of impurity-rich mattes and complexities in producing highly pure metals. They also dissolve in slags and intoxicate vicinities at which the slag is disposed.

Thus, treatment of low grade and complex sulfide ores is essential. To optimize the processes of impurity elimination from the sulfide ores acquisition of accurate thermodynamic data and knowledge of stable phase relationships at the pre-roasting conditions are required. The acquisition of experimental thermodynamic data for some conditions may lead to the determination for other conditions, computationally, by using the standard equations (1) to (8).

The pure binary sulfides in the (Fe, Ni, Cu, Zn)-S systems and their ternaries as well as the (Ni, Cu)-(As, Sb) systems are discussed in the previous reports [1, 2]. The main purpose of this study was to review stable phase relations in the (Ni, Cu)-(As, Sb)-S, Cu-Bi-S and Zn-As-S systems and their thermodynamic properties at the presence of the impurities. In spite of the complex nature of phase equilibria and thermodynamics in these systems, equilibrium phase relations and thermodynamic data for some phases are reviewed, even though far from complete.

1.1 Thermodynamics of Regular Solutions

The heat capacity of a homogenous phase in a certain temperature range is generally described by equation (1) [3].

$$C_P = a + b \cdot T + c \cdot T^{-2} + d \cdot T^2 \qquad (1)$$

where coefficients a, b, c and d are experimentally determined. As temperature changes if a phase change occurs, the new heat capacity for the new phase and temperature range is expressed as:

$$C'_P = a + b \cdot T' + c \cdot T'^{-2} + d \cdot T'^2 \qquad (1.1)$$

Within the stability temperature range of the homogenous phase the enthalpy, entropy and Gibbs free energy of the phase can be calculated from the equation (1) using equations (2), (3) and (4), respectively [3].

$$H(T) - H(25°\text{C}) = \int_{25°\text{C}}^{T} C_P dT + \sum \Delta_{tr} H \qquad (2)$$

$$S(T) - S(25°\text{C}) = \int_{25°\text{C}}^{T} \left(\frac{C_P}{T}\right) dT + \sum \Delta_{tr} S \qquad (3)$$

$$S(T) = \int_{0}^{25°\text{C}} \left(\frac{C_P}{T}\right) dT + \int_{25°\text{C}}^{T} \left(\frac{C_P}{T}\right) dT \qquad (3.1)$$

$$G(T) = H(T) - T \cdot S(T) \qquad (4)$$

where $\Delta_{tr}H$ and $\Delta_{tr}S$ are enthalpy and entropy of phase transformation(s), respectively. When considering non-ideal mixing of phases A and B intermolecular forces A-A, B-B and A-B that are all different from each other emerge. This causes change in volume of the solution from cumulative value of the solutes. Therefore, there will be a contribution to the various thermodynamic parameters for mixing due to these differences. Mixing energy (G_M) of the two component solid solution following the regular behaviors can be expressed as:

$$G_M = \omega X_A X_B + RT(X_A lnX_A + X_B lnX_B) \quad (5)$$

where ω is regular solution models parameter. The first term in equation (5) is called the excess Gibbs energy of mixing. For a multi-component system the general formula for G_M is written as:

$$G_M = \mathrm{G} - \sum X_i \mu_i^o = \sum X_i \bar{G}_i \quad \rightarrow$$

$$G_M = \mathrm{RT} \sum X_i lna_i \quad (6)$$

where G is the Gibbs energy of the system, G_i is the partial molar Gibbs energy
of mixing (the difference between component i's contribution to G in the mixture versus pure i) and a_i is activity of component i in the system. In a similar fashion, the entropy of mixing and enthalpy of mixing are given as:

$$H_M = \mathrm{H} - \sum X_i H_i^o \quad (7)$$

$$H_M = \omega_{\mathrm{ij}} X_i X_j \quad (7.1)$$

$$S_M = \mathrm{S} - \sum X_i S_i^o \quad (8)$$

$$S_M = -\mathrm{R} \sum X_i \, lnX_i \quad (8.1)$$

2 Binary Systems

This section covers thermodynamic properties and phase equilibria of the impurity sulfides (As-S, Sb-S and Bi-S) exclusively, based on the available literature data.

2.1 As-S System

At 1 atm arsenic sublimes at 615°C and at 36 atm it melts at 814°C (Appendix A). Contrary to Bi and Sb, the melting temperature of As increases with increasing pressure [4]. Realgar (AsS) and orpiment (As_2S_3) melts at 319 ± 2°C and 310 ± 2°C [5, 6, 7], respectively. As shown in Figure 1, between 321°C to 814°C the only condensed phases in the As-S system are metallic arsenic and an As-S liquid(s). The composition of As-S liquid in equilibrium with metallic arsenic at 600°C is 77.2 ± 0.1 wt. % As, and the maximum arsenic content of the As-S liquid at 700°C is about 82.7 ± 0.8 wt. % As [6]. As a result of an experimental work at different pressure and temperature conditions, Emelina et al. [7] reported that a metastable phase As_2S_5 exists at moderate pressures, its standard heat of formation is given in Appendix C. αAs_2S_3, αAs_4S_4 and As_4S_3 are known to sublime congruently. They also melt congruently. Mass spectroscopic analysis of the gas phase over αAs_2S_3 suggests that the total pressure over αAs_2S_3 can be expressed as [7]:

$$\log(p\ in\ Pa) = -\frac{8000\ \pm 150}{T} + (15.07 \pm 0.1) \qquad \text{(for } 430 < T(K) < 500\text{)} \qquad (9)$$

and the total pressure over αAs_4S_4 as [7]:

$$\log(p\ in\ Pa) = -\frac{6610 \pm 200}{T} + (13.67 \pm 0.1) \qquad \text{(for } 450 < T(K) < 500\text{)} \qquad (10)$$

The saturated vapor pressures over the αAs_2S_3 and αAs_4S_4 as determined by Emelina et al. [7] are shown in Table 1. The four eutectic points of the As-S system, partly shown in Figure 1, are listed in Table 2.

Table 1. Saturated vapor pressures in the As-S system; P_1, calculated by thermodynamic modeling, p_2, evaluated from experimental data [7].

Equilibrium phases	T (K)	p_1(Pa)	p_2(Pa)
$S_{\alpha As4S4}$,V	473	0.5	0.5
	540	30.4	26.9
$S_{\alpha As2S3}$,V	571	12.4	11.5
$S_{\alpha As2S3}$,V,$S_{\alpha As4S4}$	470	0.4	0.4
	500	2.9	2.6
$S_{\alpha As2S3}$, $S_{\alpha S}$ V	350	0.1	0.1

Table 2. The four eutectics invariant equilibria in the As-S system [7].

Composition of S	Eutectic T(°C)
0.42	196.85 ± 4
0.438	199.85 ± 4
0.56	297.85 ± 4
~1	115.85 ± 4

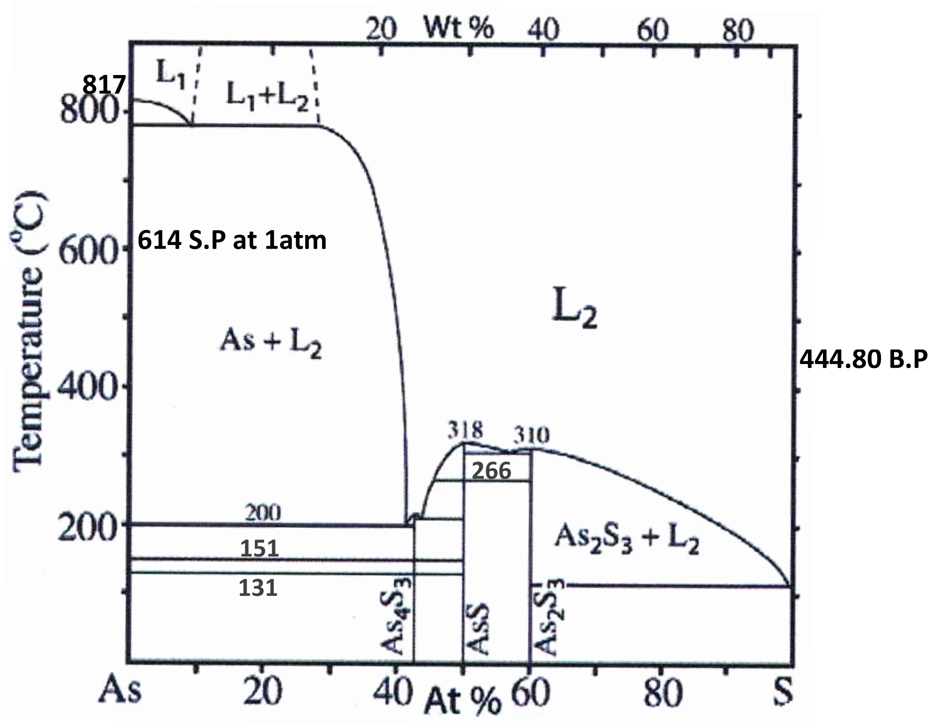

Figure 1. A condensed As-S phase diagram (modified from Massalski et al. 1990) [5].

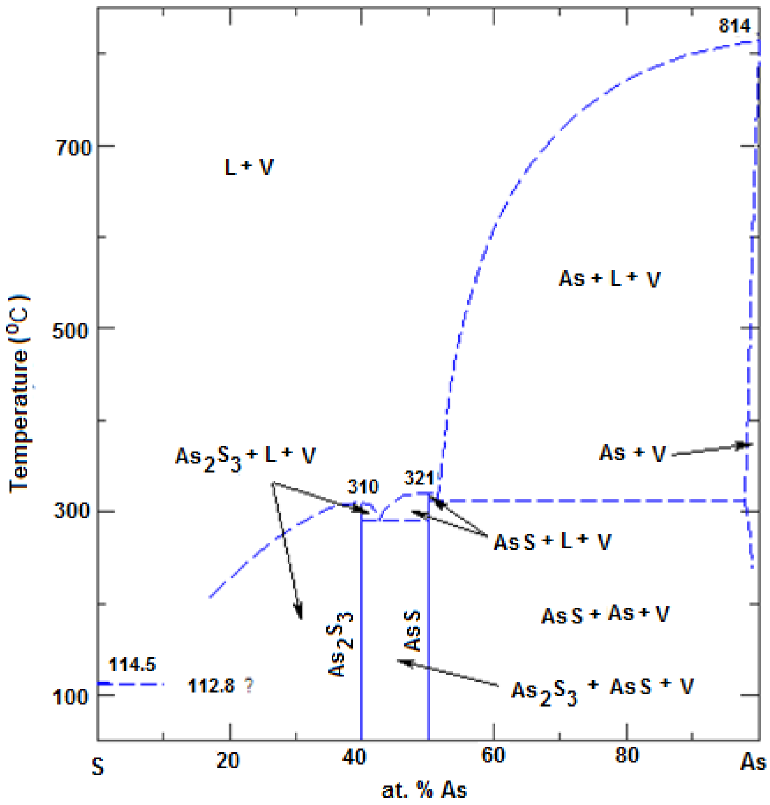

Figure 2. The As-S phase diagram [8].

From Figure 3 (b) and Figure 4 it is possible to infer that the decomposition of sulfosalts, which contain As, to form As-S melts can be constrained at the presence of PbS and Bi_2S_3. Apart from the melting temperature of pure S (which occurs at 113°C), the first melt in the (Fe/Ni/Cu/Zn)–As–S systems appears at 281°C [4]. It forms at the eutectic between realgar (AsS) and orpiment (As_2S_3). The melt field expands rapidly with increasing T; and by 321°C, the whole join from realgar to sulfur is a melt (Hall & Yund 1964) [4]. As it is shown in Figure 3 (a), at 550^{o}C the (AsS, As_2S_3)-Pb joins lies totally under the liquid region and the (AsS, As_2S_3)-PbS joins contain some amount of galena at the PbS-rich corner.

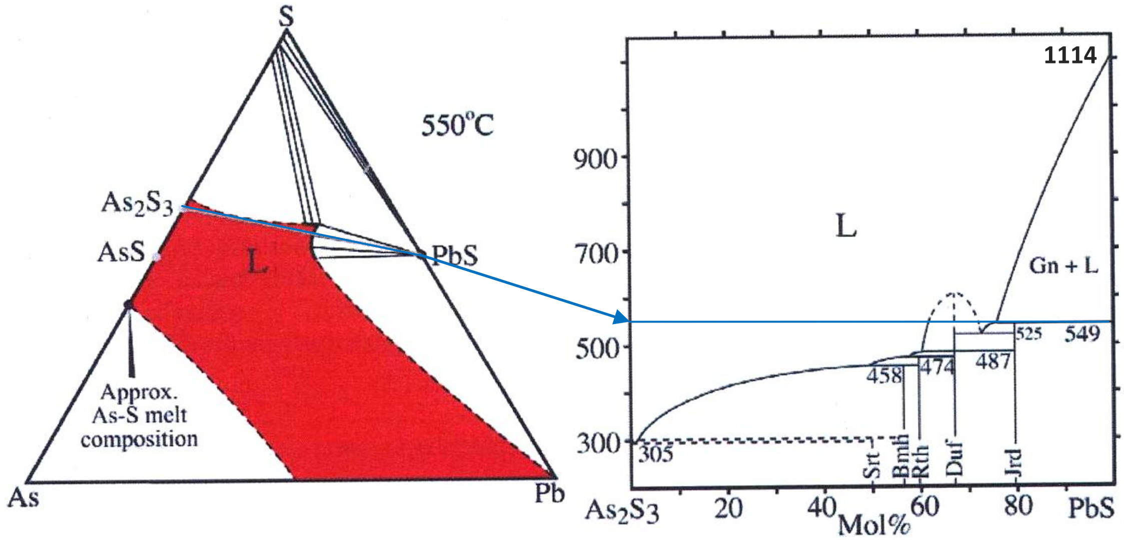

Figure 3. a) Isothermal section of the As-Pb-S system. b) As_2S_3-PbS system (modified from Kutolglu, 1969) [5].

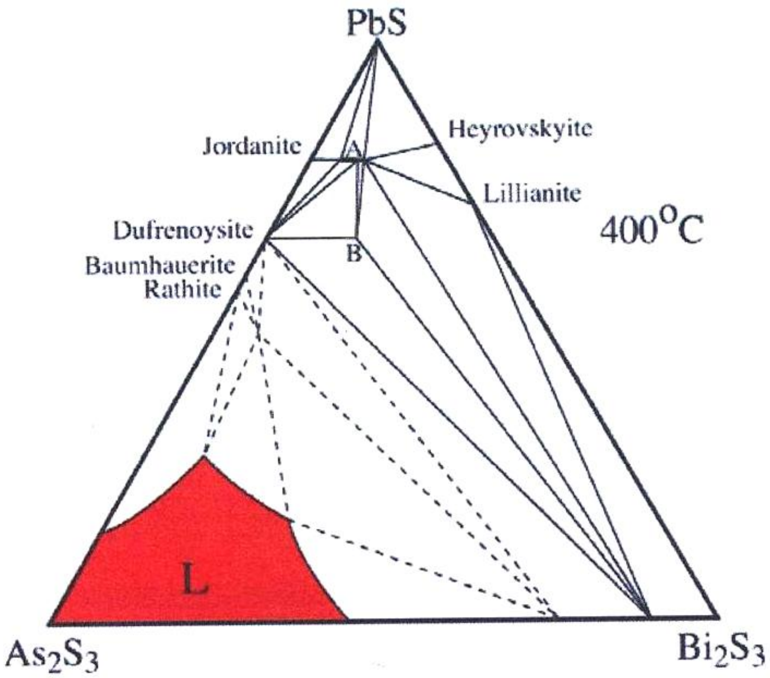

Figure 4. Isothermal section of the As_2S_3-Bi_2S_3-PbS system at 400^{o}C (after Walia and Chang, 1973) [5].

2.2 Sb-S System

As indicated in Figure 5, at standard conditions, Sb melts at about 631^{o}C. Contrary to most metal/metalloids, its melting temperature decreases with increasing pressure; this pressure dependency can be approximated to be –0.2°C/kbar (Liu & Bassett, 1986) [4]. Thus, for Sb-bearing systems, increasing pressure may actually decrease their melting temperatures, even though not as large as for Bi-bearing systems (discussed in section 2.3). This system is characterized by liquid immiscibility regions and stibnite, Sb_2S_3, is the only condensed stable binary phase. Stibinite is very common among natural minerals, with noncomplex inversions and solid solutions [9]. Its standard state heat of formation is -147 kJ/mol [10], values obtained from other sources are shown in Appendix C. As shown in Figure 5, Sb_2S_3 congruently melts at 550^{o}C, which is 6^{o}C less than the value given by Skinner et al. [9]. Its standard state Gibbs energy of formation below 600^{o}C is shown in Appendix E.

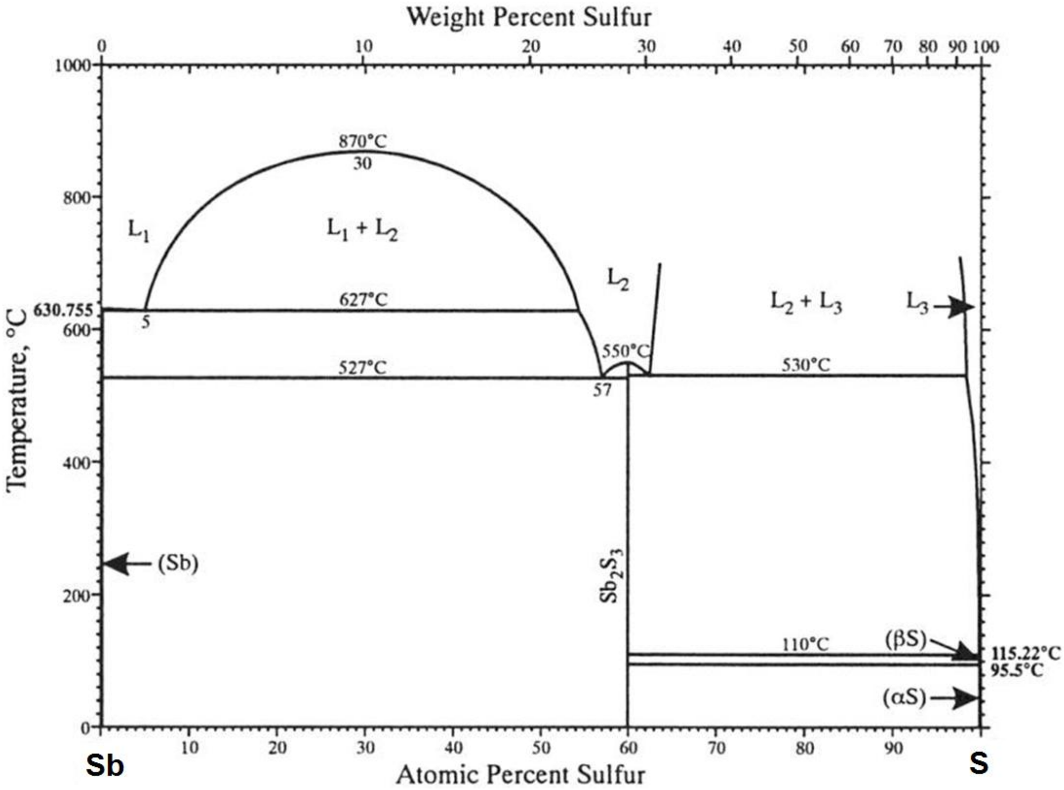

Figure 5. A condensed Sb -S phase diagram [11].

Figure 6 shows that by 500°C most of the area in the As-Sb-S system bounded by stibnite (Sb_2S_3), realgar(AsS), and sulfur is molten.

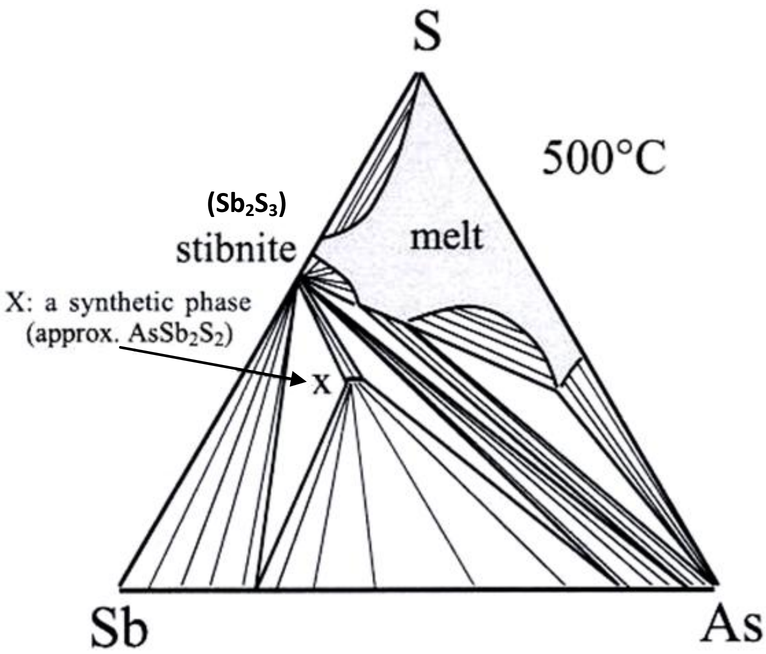

Figure 6. A one bar phase relations in the As-Sb-S system at 500°C (after Luce et al., 1977) [4].

2.3 Bi-S System

As indicated in Figure 7, at normal conditions, Bi melts at about 271°C. Contrary to most metal/metalloids, its melting temperature decreases with increasing pressure; the pressure dependency can be approximated to be –4.5°C/kbar (Liu & Bassett, 1986) [4]. Thus, for Bi-bearing systems, increasing pressure may actually decrease their melting temperatures. Stoichiometric binary phases in the system include; Bi_2S_3 (bismuthinite), Bi_4S_3 (ikunolite), BiS, Bi_2S, Bi_3S_2 as well as compositions approximating to Bi_3S_5 and Bi_3S_4, as reported from Kazakhstan (Pavlova, 1988). However, synthetic works in the system have produced only a single binary phase Bi_2S_3 [12].

As Figure 7 shows the intermediate compound Bi_2S_3, which forms at 60 at. %S, melts at 775°C [13]. The standard Gibbs energy of formation of this compound, according to equation (11) at 510°C, is about -137 kJ/mol. [14] and for T < 300°C it is shown in Appendix E. Table 3 shows the standard state thermodynamic properties, which are also indicated in Appendix C as suggested by another source. The Bi- Bi_2S_3 region of the phase diagram contains an eutectic close to Bi, whereas the Bi_2S_3-S region has a miscibility gap in the liquid, resulting in monotectic reaction, and an eutectic close to pure S.

$$2Bi + 3/2S_2(g) = Bi_2S_3 \qquad \Delta G^o(510^oC) = -136.8 \pm 4 \text{ kJ/mol of } Bi_2S_3 \qquad (11)$$

Table 3. Standard thermodynamic properties of Bi_2S_3 [15, 16].

composition	ΔH_f^o(KJ/mol)		ΔS_f^o(J/mol.K) 273.15K	ΔC_p^o(kJ/mol.K) 273.15K	ΔG_f^o(kJ/mol) 273.15K
	273.15K	298.15K			
Bi_2S_3 (Bismuthinite)	-143.1	-184.1	200.4	122.2	-140.6
Bi	0		56.7	25.5	-

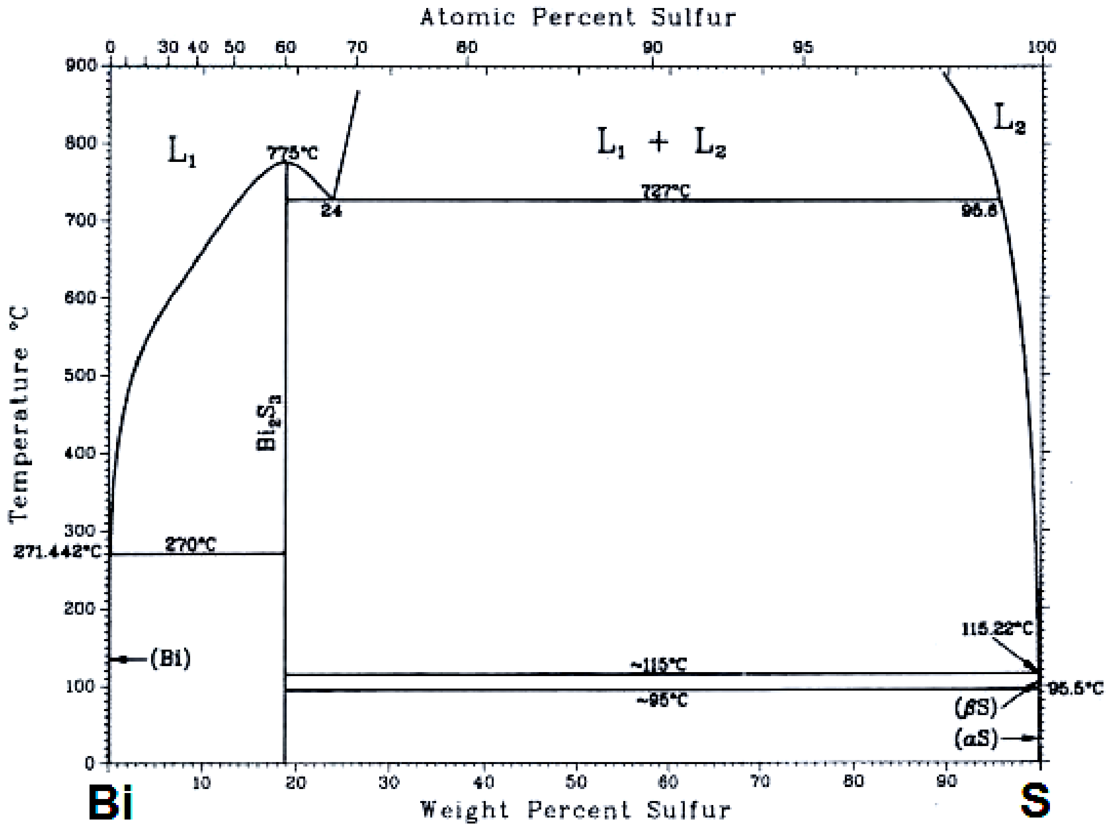

Figure 7. The Bi-S phase diagram; Bi_2S_3 contains 19 wt. % S [17].

3 Ternary and 'Quaternary' Systems

In this section thermodynamics and phase equilibria of the Cu-(As,Sb)-S, Ni-(As,Sb)-S and Zn-As-S systems are reviewed.

3.1 Ni-As-S System

The compositional phase relations in the Ni-As-S system are illustrated in Figure 8. The only identified ternary phase in this system is NiAsS (gersdorffite) [6]. It has a pyrite (Pa3) like crystal structure. Yund's [6] experimental studies on the stable phase relations in the Ni-As-S system, using silica-glass techniques, are illustrated in Figure 9, Figure 10 and Figure 11. The gas vapor was reported to be stable in all assemblages even though the gas compositions were not determined.

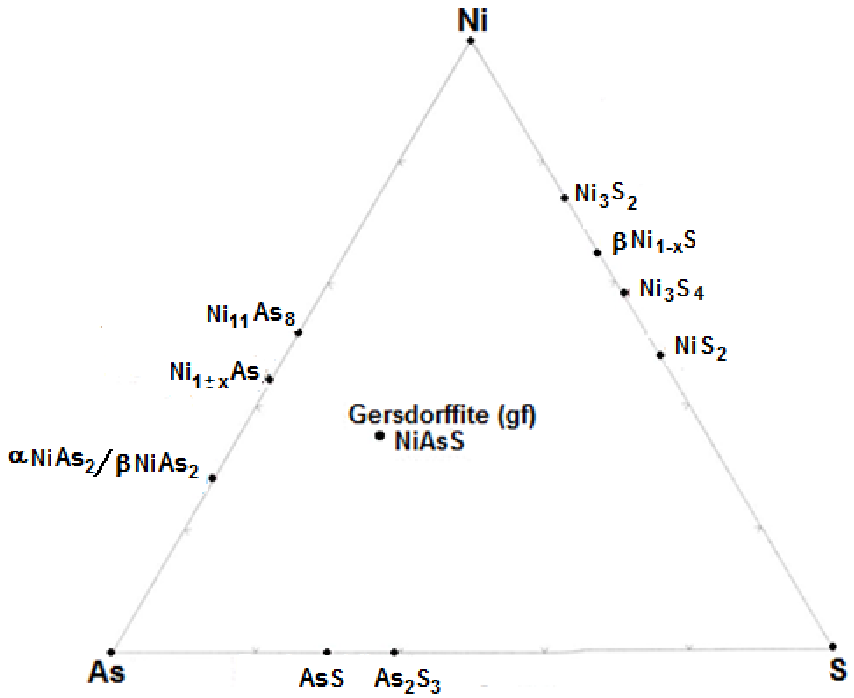

Figure 8. Minerals in the Ni-As-S system, only the ideal stoichiometric compositions are shown [6].

Natural assemblages of nickel sulfide and arsenide minerals correspond closely to the stable assemblages in the isothermal section shown of Figure 9, for instance $NiAs_2$-$NiAs_{2-x}S_x$-As-vapor.

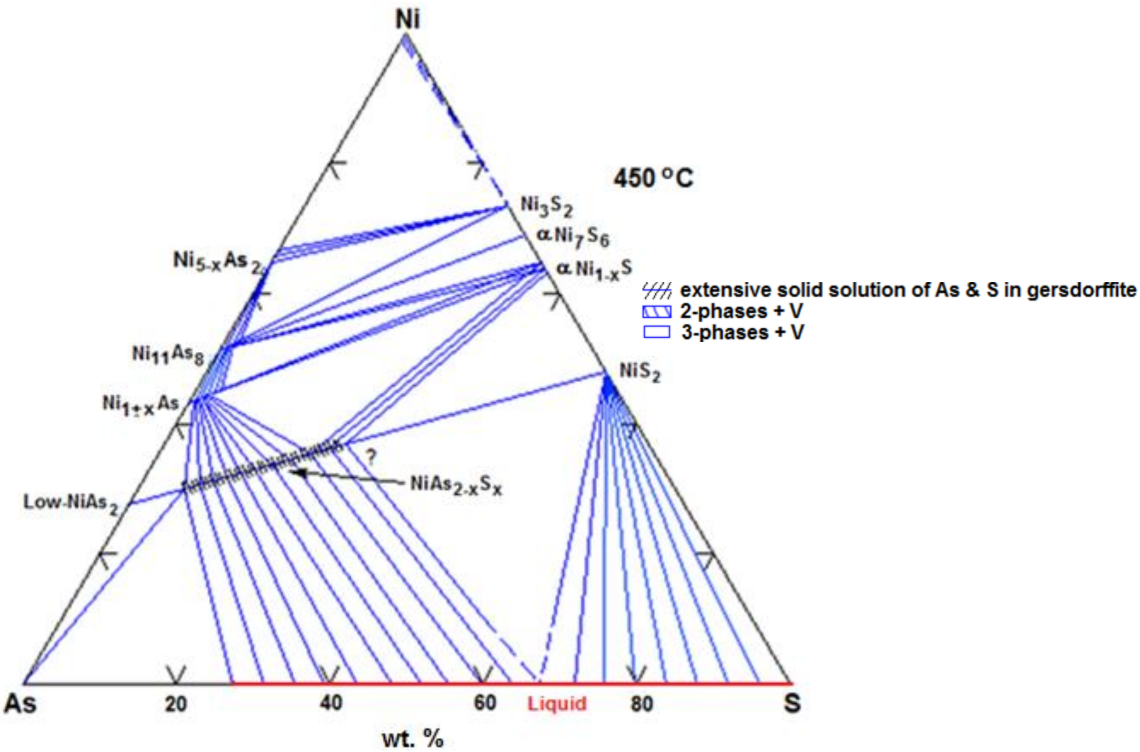

Figure 9. Isothermal section of the Ni-As-S system at 450°C, in the presence of vapor in all assemblages [6].

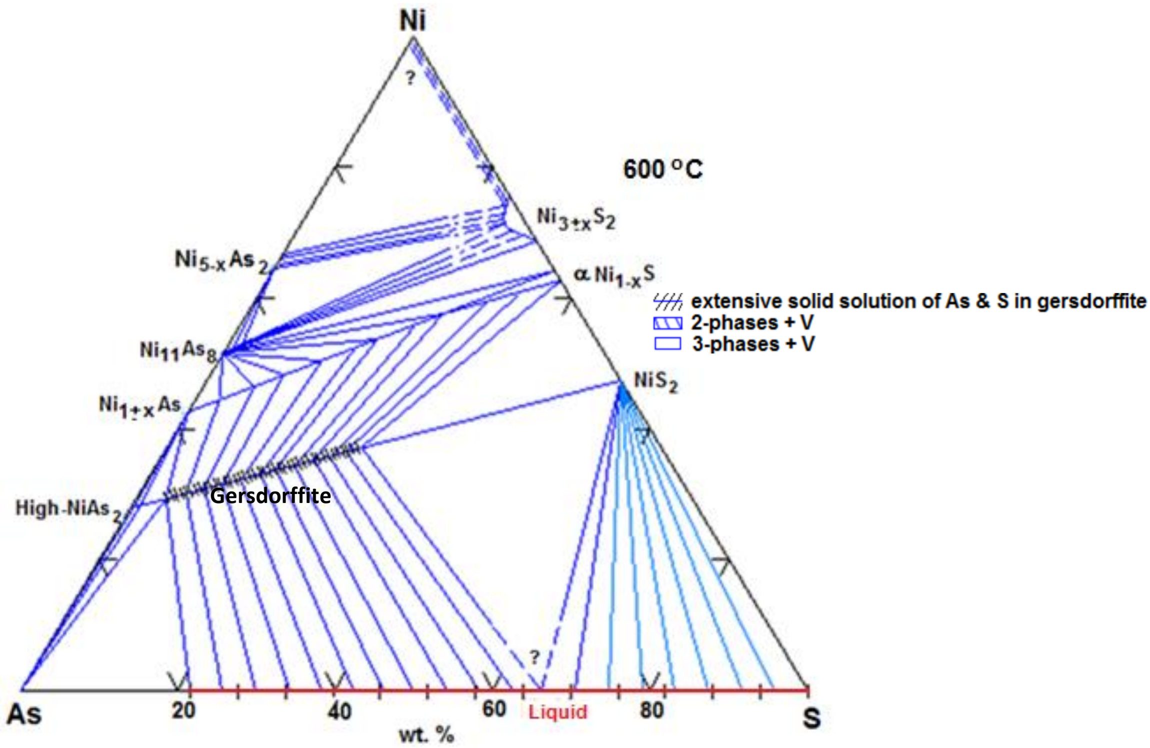

Figure 10. Isothermal section of the Ni-As-S system at 600°C [6].

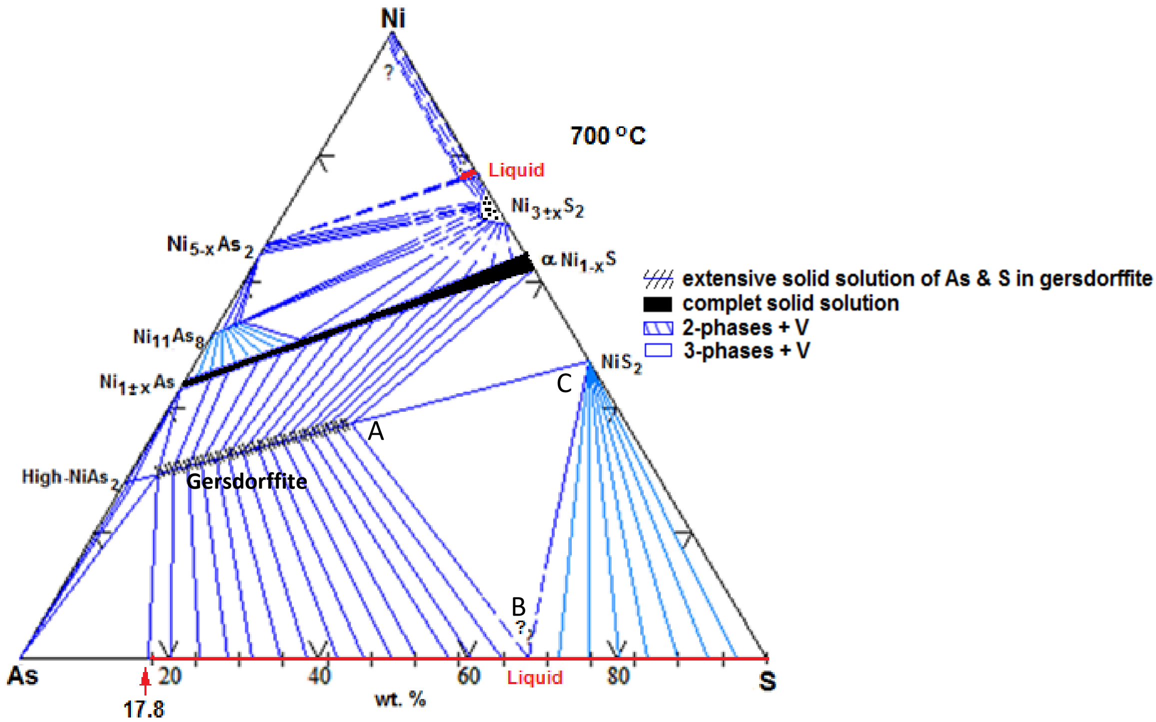

Figure 11. Isothermal section of the Ni-As-S system at 700°C [6].

Between 700°C and 600°C the principal change in the phase relations under a total pressure of 1 atm is the composition of Ni(As,S) in the assemblage Ni(As, S)-maucherite($Ni_{11}As_8$)-$Ni_{3\pm x}S_2$-vapor, as shown in Figure 11. The composition of Ni(As, S) solution in the assemblage corresponds to the formula $NiAs_{0.56}S_{0.44}$ at 700°C, whereas at 660°C the composition of Ni(As,S) in the same assemblage is $NiAs_{0.22}S_{0.78}$. With decreasing temperature the composition of Ni(As,S) in this assemblage continuously moves toward NiS, and at 600°C essentially pure NiS is the stable phase in equilibrium with $Ni_{3\pm x}S_2$ and vapor.

Below 560°C the solid solution between niccolite($Ni_{1\pm x}As$) and αNiS_{1-x} is no longer complete and the univariant assemblages niccolite-gersdorffite-αNi_{1-x}(S, As)-vapor and niccolite-maucherite-αNi(S,As)-vapor become stable. The only additional changes in these assemblages at lower temperature are a decrease in the solid solution of sulfur in niccolite and maucherite and of arsenic in Ni_{1-x}(S, As). αNi_7S_6 is stable below 573°C; this gives rise to the new univariant assemblages consisting of $Ni_{3\pm x}S_2$-$Ni_{11}As_8$-αNi_7S_6-vapor and αNiS-maucherite-αNi_7S_6-vapor as shown in Figure 9. The polymorphic inversion of the high temperature phase Ni_3S_2 to heazlewoodite (Ni_3S_2) occurs at 556°C [6]. The inversion of rammelsbergite ($\alpha NiAs_2$) to pararammelsbergite ($\beta NiAs_2$) occurs between 500°C and 450°C, when it is in equilibrium with gersdorffite and arsenic. Therefore, pararammelsbergite is the stable polymorph at 450°C (Figure 9), however, its sulfur content is too small to be shown on the phase diagram.

Figure 11 shows that 13 bivariant three phase assemblages (two condensed + V) shown by closely spaced, parallel or radiating tie lines. The dark area and the heavy dark line with scratches on it indicate that there is an extensive solid solution between $Ni_{1\pm x}As$ and $\alpha Ni_{1-x}S$ and that there is extensive solid solution of As and S in NiAsS, respectively. Nine univariant (condensed phases: Ni

(As, S) with wt. % NiS ranging from 8.49 to 91.08) four-phase assemblages (three condensed phases + V) are shown as clear areas in Figure 11. The broken lines show the approximated boundary lines.

At 700^{o}C the maximum arsenic content of gersdorffite corresponds to $NiAs_{1.77}S_{0.23}$, and the maximum sulfur content corresponds to $NiAs_{0.77}S_{1.23}$. Thus, gersdorffite solid solution extends along a line rammelsbergite ($\alpha NiAs_2$) to vaesite (NiS_2), with the largest amount of solid solution on the $NiAs_2$ side of the stoichiometric NiAsS. The difference in the As content between the two ends of this solid solution is approximately 30 wt. %.

If the substitution of arsenic and sulfur for each other is the only type of solid solution possible in gersdorffite, then the Ni/(As + S) atomic ratio should be constant and equal to 0.5. However, the As/S ratio varies largely. For instance, at 700^{o}C gersdorffite is homogenous from $NiAs_{1.77}S_{0.33}$ to $NiAs_{0.77}S_{1.23}$ and gersdorffite that is in equilibrium with $NiAs_2$ has the composition $NiAs_{1.8}S_{0.20}$ at 660^{o}C and $NiAs_{1.72}S_{0.28}$ at 450^{o}C. The difference between the two later cases is only about 2 wt. % As. According to Yund's [6] experimental results maximum arsenic content of gerdorffite occurs at 660^{o}C.

Yound [6] investigated also the solvus between NiAs and NiS by means of series exsolution experiments, using a homogenous phase Ni(*As*,S) (italics indicates larger at. %) as a starting material. His experimental results are listed in Table 5. Based on the results he conclude that the join between NiAs-NiS appears to be truly binary. The identified phase relations in the Ni-As-S system (below 700^{o}C) are shown in Table 4.

Table 4. Phase relations in the Ni-As-S system below 700^{o}C [6].

Reaction	wt. % As	wt. % S	↓T (^{o}C)	Heating time, days	Condensed phases
Ni_3S_2 + As	15.00	22.70	660	114	$Ni_{11}S_8$ + $Ni_{3\pm x}S_2$ + αNi(S,As)$^{(71 wt. \% NiS, 29 wt. \% NiAs)}$
As + S	85.00	15.00	660	2	$L_{19.9 wt.\% S}$ + As
Ni_3S_2 + AsS	8.89	27.11	640	31	$Ni_{11}S_8$ + $Ni_{3\pm x}S_2$ + αNi(S,As)$^{(78 wt. \% NiS, 22 wt. \% NiAs)}$
Ni_5As_2 + AsS	39.48	4.70	600	43	$Ni_{11}S_8$ + $Ni_{3\pm x}S_2$
Ni_3S_2 + As	15.00	22.70	600	19	$Ni_{11}S_8$ + $Ni_{3\pm x}S_2$ + αNiS
Ni_5As_2 + AsS	41.57	6.43	600	57	$Ni_{11}S_8$ + Ni(*As*,S)
Ni_5As_2 + L_{70}	32.53	23.47	600	25	αNi_{1-x}(S,As) + gersdorffite
NiS + L_{70}	5.41	41.59	600	40	αNi_{1-x}(S,As) + gersdorffite + NiS_2
$NiAs_2$ + AsS	71.55	5.00	600	18	$\alpha NiAs_2$ + gersdorffite + As
As + S	85.00	15.00	600	2	$L_{(22.9 wt.\% S)}$ + As
Ni_3S_2 + As	15.00	22.70	500	37	$Ni_{11}S_8$ + αNi_7S_6 + αNiS
$Ni_{11}As_8$ + Ni(As, S)	41.57	6.43	500	46	$Ni_{11}S_8$ + $Ni_{1\pm x}S$ + αNi(S,As)
Ni(S, As) + AsS	34.90	21.10	500	36	$Ni_{1\pm x}S$ + αNi_{1-x}(S,As) + gersdorffite
$Ni_{11}As_8$ + As + S	81.60	8.00	450	49	$\beta NiAs_2$ + gersdorffite + As
NiS + AsS	13.00	34.34	280	50	gersdorffite + $\beta Ni_{1-x}S$ + $\beta NiAs_2$

Table 5. NiAs-NiS solvus; starting material was a homogenous Ni(*As*, S) in which 53.78 wt. %NiS and 46.22 wt. %NiAs [6].

Heating time, days	T (^{o}C)	Ni(*As*, S) wt. %NiS	Ni(S, As) wt. %NiS
63	600	No change	
31	590	29.3	70.6
31	585	27.1	74.3
28	550	17.5	82.5
21	500	10.8	90.7
63	500	10.5	90.2
30	400	12.5	96.2
109	400	10.4	96.5
213	400	9.3	96.7
650	400	7.2	96.7
190	300	~26	85
570	300	~9	α-Ni(S, As)

By determining the vapor pressure of the gas (2S(l) = S_2(g) & 4As(l) = As_4(g)) in equilibrium with the condensed phases in the triangle A-B-C, in Figure 11; Lynch [18] represented the equilibrium reaction in the field as reaction (12) and calculated the Gibbs energy of the reaction (12) as expressed in equation (I).

(η)NiS_2(s) + ¼As_4(g) = NiAsS(S-rich part) + ½S_2(g) ΔS^{o}=2.1J/g.mol.K (calculated)   (12)

$$\Delta G_r(\text{J/g.mol.}) = -\,RT\cdot\left(\frac{4275}{T}+0.249\right) \qquad 825 < T(K) < 975 \qquad \text{(I)}$$

The calculated entropy of reaction (12) is very small, however, this is not unexpected when gaseous species are consumed and produced in the reaction [18]. By combining the calculated entropy for reaction (12) and literature values for As_4, S_2 and NiS_2 the standard entropy of NiAsS is determined to be 250 J/g. mol. K.

Adding the calculated Gibbs energy for reaction (12) and the literature value for reaction (13), i.e. equation (II), Lynch [18] estimated the standard energy of formation of gersdorffite (S-rich), according to reaction (14), as expressed in equation (III).

Ni(s) + S_2(g) = NiS_2(S)   (13)

ΔG^{o}(J/g.mol.) = - 85670 + 56.777·T   for 675 < T(K) < 1070   (II)

Ni(s) + ¼As_4(g) + ½S_2(g) = NiAsS   (14)

ΔG^{o}(J/g.mol.) = -121000 + 54.7·T   for 825 < T(K) < 975   (III)

3.2 Ni-Sb-S System

Major natural minerals in this system include vaesite (NiS_2), zlatogorite ($CuNiSb_2$), ullmannite (NiSbS/(Ni,Fe,Co)(Sb,As)S), willyamite ((Ni,Co)SbS), breithauptite (NiSb) and nisbite ($NiSb_2$). A micro assemblage of NiSb, $NiSb_2$ and NiSbS in Pirrotinovaya and Pyataya Elektricheskaya gold ore veins are illustrated in Figure 12.

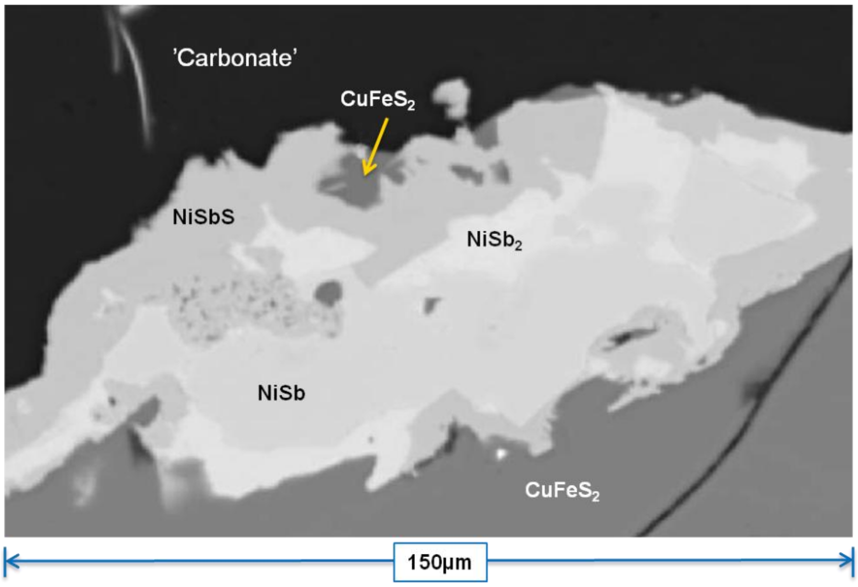

Figure 12. Backscattered electron micrograph showing an intergrowth of phases in the Ni-Sb-S system in between chalcopyrite and carbonate [19].

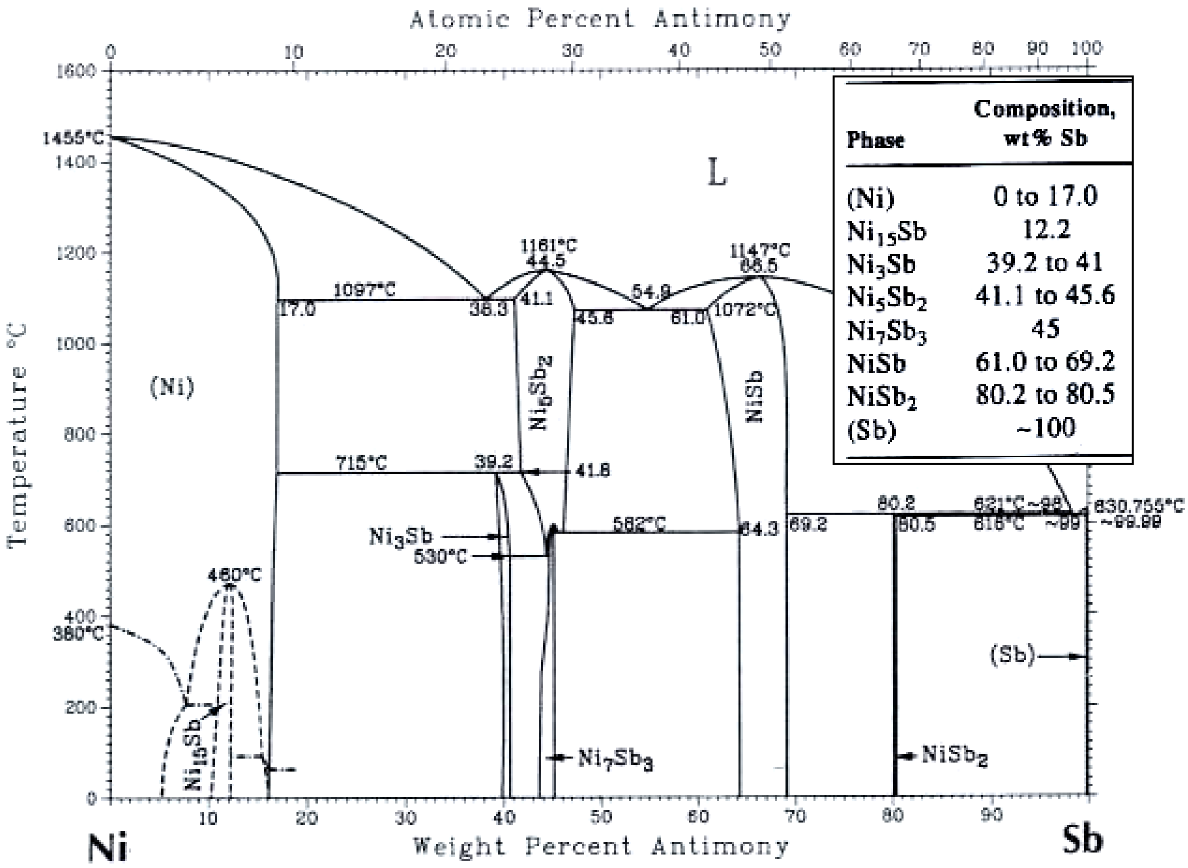

Figure 13. The Ni-Sb phase diagram (G. H Cha, S. Y Lee, P. Nash, 1991) [17].

The reaction scheme of Lange and Schlegel (1951) [16] for the Ni-Sb-S system, shown in Appendix B, indicates that the stoichiometric composition of ullmannite (NiSbS) is Ni:Sb:S = 1:1:1. Bayliss's [20] experimental studies to determine compositional limits of ullmannite (NiSbS) and cobaltite (CoAsS) showed that an extensive substitution of Co for Ni results in a variety of cobaltian ullmannite, (Ni, Co)SbS, and extensive substitution of As for Sb results in a variety of arsenian ullmannite, Ni(As, Sb)S. Experimental results, where $Ni(Sb, As, S)_2$ mixtures were heated at 550°C for one month, are shown in Figure 14, as a ternary NiS_2-$NiSb_2$-NiAs system.

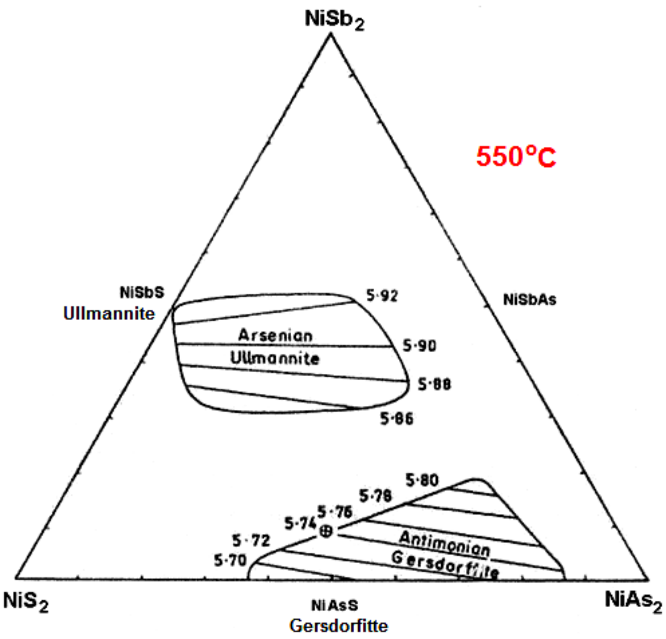

Figure 14. A ternary diagram of the NiS_2-$NiAs_2$-$NiSb_2$ system showing the limits of solid solution at 550°C and associated cell dimensions (Å) [20].

Antimonides of Ni (e.g: nisbite, $NiSb_2$) appear at a very low activity of S and As [19]. In some gold deposits nisbite occurs among native antimony in association with cuprostibite Cu_2Sb, zlatogorite $CuNiSb_2$, galena, ullmannite (Ni,Fe,Co)(Sb,As)S, seinajokite $FeSb_2$, gudmundite FeSbS, and native lead. Bryzgalov's et al. [19] study of antimonides of Ni and Au in gold ore veins showed that nickel antimonides, not larger than 0.1 mm in size, have a nearly stoichiometric composition.Their analytic studies also showed that ullmannite ('NiSbS') has the formula: $(Ni_{1.03}Fe_{0.04})_{0.97}(Sb_{1.01}As_{0.01})_{1.02}S_{1.01}$, breithauptite ('NiSb') has the formula: $(Ni_{0.97}Cu_{0.01}Fe_{0.01})_{0.99}(Sb_{1.00}S_{0.01})_{1.01}$ and nisbite ('$NiSb_2$') has the formula: $Ni_{0.97}(Sb_{1.97}As_{0.02}S_{0.04})_{2.03}$. The composition of ullmanite, as reported from different ore deposits, is summarized in Table 6. NiSb, which melts at 1158°C, may dissolve < 1 %PbS, but PbS may dissolve up to 3%NiSb, as shown in Figure 15.

Table 6. Compositions (wt. %) of ullmannite from different ore deposits [21].

	Ni	Co	Fe	Sb	As	Bi	S
Gosenbach, Germany	28.91	1.13	0.40	42.93	10.28	0.68	16.22
Petersbach mine, Germany; by electron microprobe	27.3	0.8		52.8	3.5	1.0	15.1
Broken Hill, Australia; by electron microprobe	23.3	3.8		58.9	0.4		14.8
NiSbS	27.62			57.29			15.09

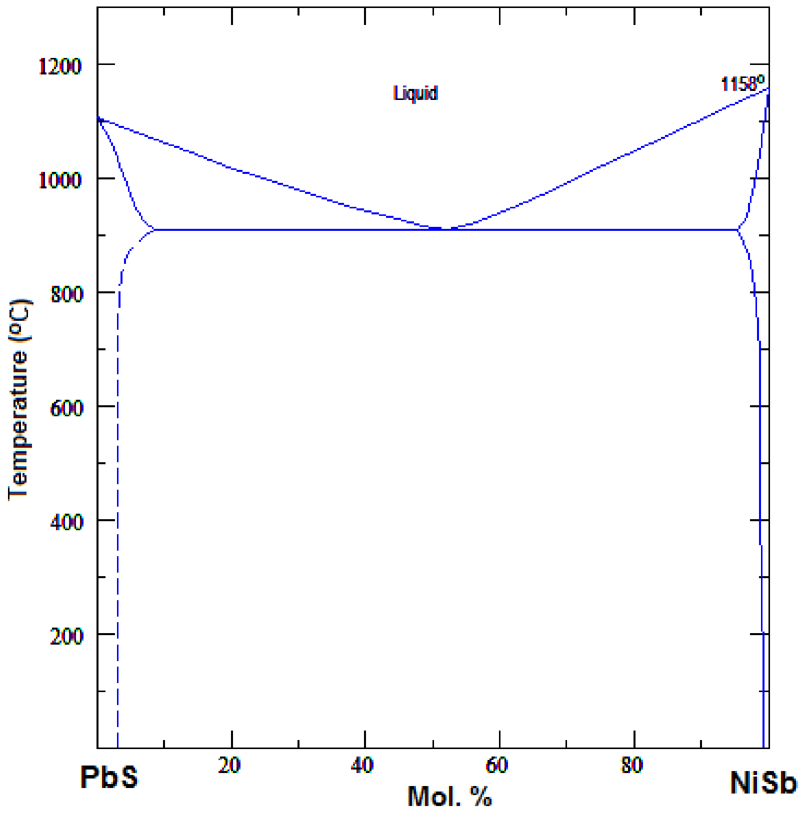

Figure 15. Phase diagram of the PbS-NiSb system [8].

Table 7. Gibbs energies of reaction of sulfosalts and their Gibbs energies of formation from the elements (standard states: Cu(s), Bi (l) and S_2 (g) at 1atm), at 400°C [28].

Phase	Reaction(1)	ΔG_r(kJ/mol) reaction (1)	Reaction (2)	ΔG_f(kJ/mol) reaction (2)
$Ni_3Bi_2S_2$	$\frac{1}{2}Ni_3Bi_2S_2 + S_2 = \frac{1}{2}Bi_2S_3 + \frac{3}{2}NiS$	-6.16	$3Ni + 3Bi + S_2 = Ni_3Bi_2S_2$	-14.01
NiSbS	$\frac{4}{3}NiSbS + S_2 = \frac{4}{3}NiS + \frac{2}{3}Sb_2S_3$	-4.96	$Ni + Sb + 1/2S_2 = NiSbS$	-7.01

3.3 Cu-As-S System

The system is characterized by three miscibility gaps and in total six ternary compounds, Cu_3AsS_4 (enargite/luzonite), $Cu_{12+x}As_{4+y}S_{13}$(tennantite), $Cu_4As_2S_5$, $Cu_6As_4S_9$, and CuAsS (lautite) [22]. The primary crystallization fields of $Cu_{2-x}S$, As, Cu_3AsS_4, and $Cu_{12+x}As_{4+y}S_{13}$ dominate the Gibbs triangle in Figure 17. The sections As–Cu_2S, As–Cu_3AsS_3, Cu_2S–Cu_3As, and Cu_2S–As_2S_3 are reported by different researchers as quasibinaries [23]. All compounds but $Cu_4As_2S_5$ exist as minerals, which are characterized by covalent As–S bonds and which crystallize in superstructures of the sphalerite or wurtzite type [22]. The structure of enargite is characterized by AsS_4 tetrahedra, whereas the compounds on the section Cu_2S–As_2S_3 contain trigonal AsS_3 pyramids. Cu_3AsS_4 has two crystal forms. The high-temperature form (enargite, en) is orthorhombic, and the low-temperature form (luzonite, lz) is tetragonal. The transition temperature is between 275 and 300°C. At higher temperatures the orthorhombic Cu_3AsS_4, enargite, has a small homogeneity range [23]. Its equation of formation energy (for both crystal forms) in the range 25-500°C is shown in Table 11. The melting behavior is not clear, the available thermal data in the literature are shown in Appedix A. $Cu_{12}As_4S_{13}$ (tennantite, tn) is body-centered cubic (bcc) with 58 atoms in the unit cell and is isomorphous with $Cu_{12}Sb_4S_{13}$ (tetrahedrite, td). It has a small homogeneity range as given by $Cu_{12+x}As_{4+y}S_{13}$ where $0 < x < 1.72$; $0 < y < 0.08$ [22]. $Cu_6As_4S_9$ (sinnerite, sin) is triclinic. $Cu_{12+x}As_{4+y}S_{13}$, tennantite, and its multinary varieties are widely spread in nature. Since the compound contains the monovalent Cu(I) and divalent Cu(II), it is better represented by the formulae $Cu(I)_{10}Cu(II)_2As_4S_{13}$ [24].

$Cu_4As_2S_5$ has a narrow homogeneity range and decomposes peritectically at 597°C into $Cu_{12+x}As_{4+y}S_{13}$ and melt [22]. Synthetic $Cu_6As_4S_9$ corresponds to the mineral sinnerite. The compound decomposes at 530°C into $Cu_4As_2S_5$ and melt. CuAsS (lautite, lt) has orthorhombic symmetry [22, 25]. In the structure, all atoms are tetrahedrally co-ordinated such that covalent bonds between the arsenic atoms result in zigzag chains of this element [2]. The stoichiometric compound melts peritectically and may decompose at 596 °C into arsenic and melt, and according to Maske and Skinner [4] at 574 °C into $Cu_{12+x}As_{4+y}S_{13}$ + As + melt. Figure 16 shows the position of all relevant compounds in the Gibbs triangle. At all temperatures between 300 and 600 °C, tie-lines exist between As and Cu_9S_5 (digenite) or Cu_2S (chalcocite) [22].

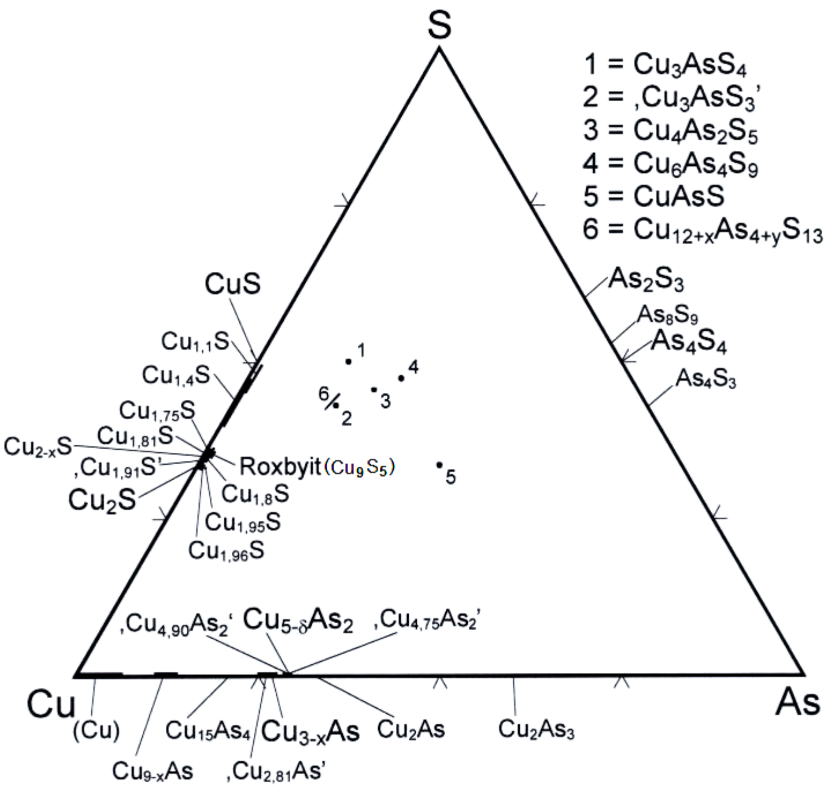

Figure 16. Compounds and their homogeneity range in the Cu-As-S system [26].

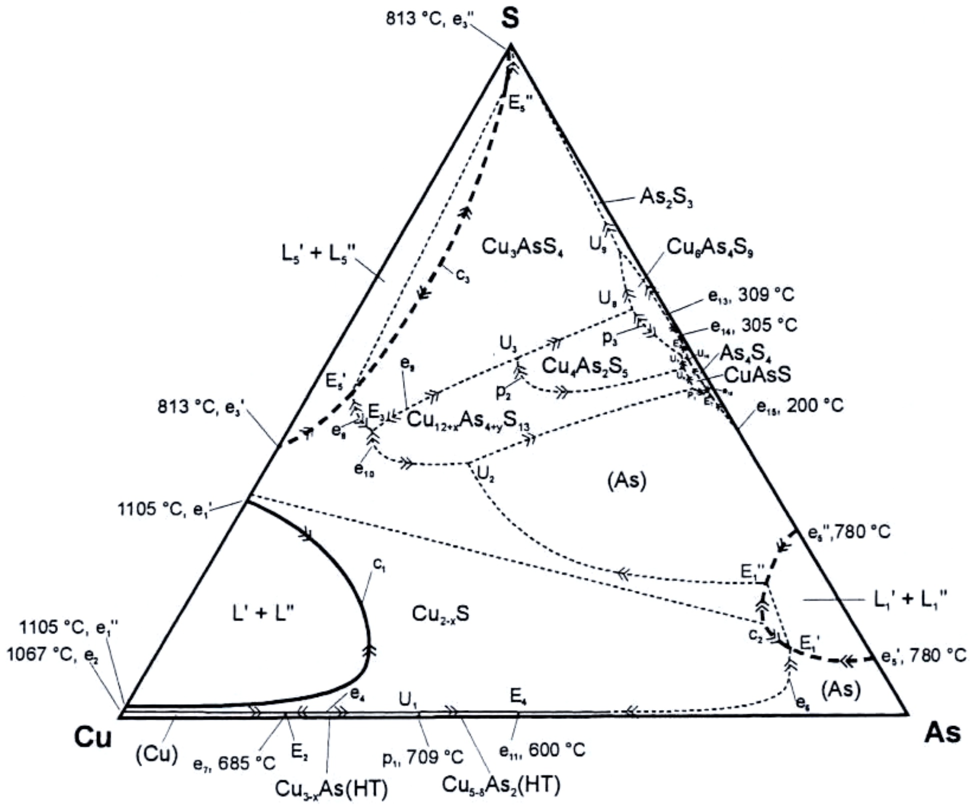

Figure 17. Liquidus projection of the Cu-As-S system [23]; the abbreviations are explained in Appendix D.

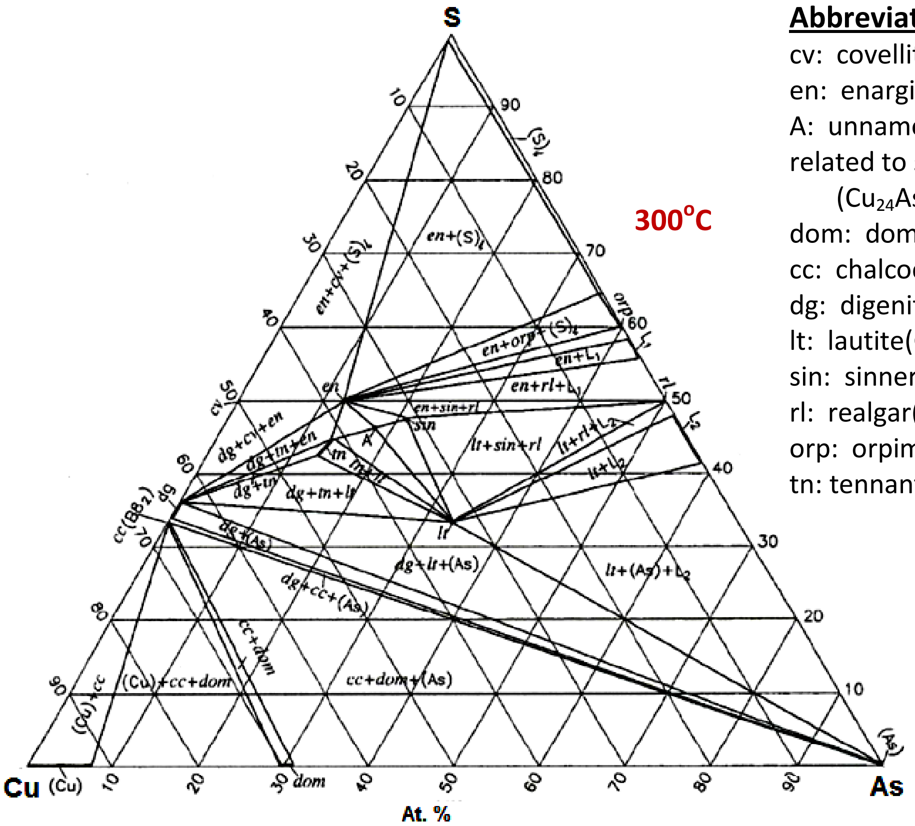

Abbreviations:

cv: covellite(CuS)
en: enargite(Cu_3AsS_4)
A: unnamed ('structurally related to sin & tn') ($Cu_{24}As_{12}S_{31}$)
dom: domeykite(Cu_3As)
cc: chalcocite (Cu_2S)
dg: digenite (Cu_9S_5)
lt: lautite(CuAsS)
sin: sinnerite($Cu_6As_4S_9$)
rl: realgar(AsS)
orp: orpiment(As_2S_3)
tn: tennantite($Cu_{12+x}As_{4+y}S_{13}$)

Figure 18. Isothermal section of the Cu-As-S system at 300°C; the narrow two-phase regions are omitted [22].

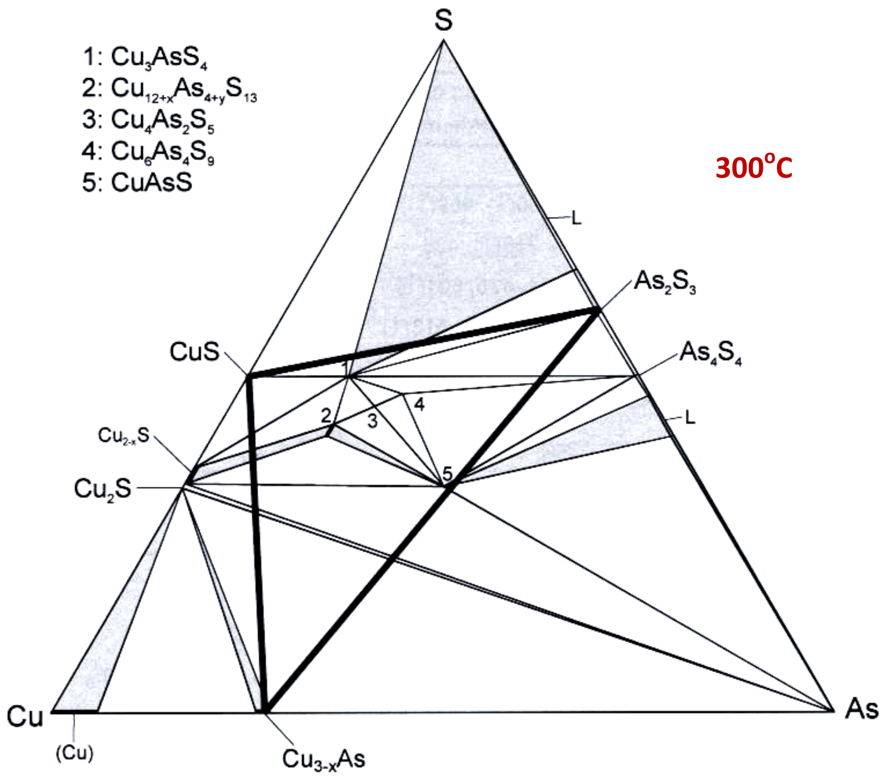

Figure 19. Isothermal section of the Cu-As-S system at 300°C [26], the same as Figure 18 but depicting the region bounded by CuS-$Cu_{3-x}As$-As_2S_3.

In the bold-line bounded region of Figure 19, Muller and Blachnik [23] made a thermal experiment and reported results in Table 8. By the thermal experiment of reaction mixture CuS and As_4S_4, they also observed that by 495°C CuS reacts with an intermediate phase $Cu_6As_4S_9$ to form enargite (Cu_3AsS_4).

Table 8. Thermal experiments and corresponding products [23].

Reaction (wt. %)	Temperature of exothermic effect (°C)	Identified phases by XRD (phases in order of intensities of reflection)
CuS(65) + As_2S_3(28) +$Cu_{3-x}As$(7)	322, 436 (small peak in DTA curve), 513 (largest peak in DTA curve)	Cu_3AsS_4, $Cu_{12+x}As_{4+y}S_{13}$, $Cu_4As_2S_5$(low in concentration)

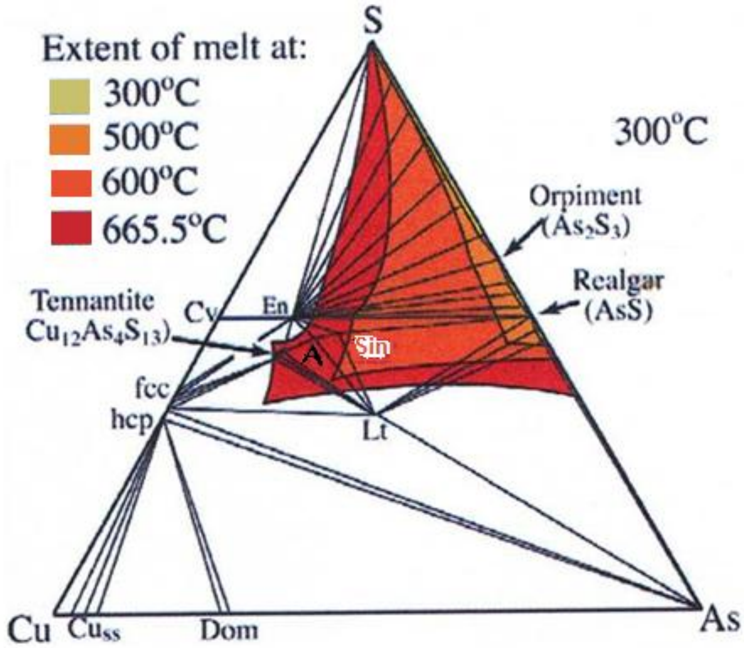

Figure 20. Isothermal section of the Cu-As-S system showing the distribution of mineral phases and melts at 300°C, compositions are in mol. %, the distribution of melts at 500°C, 600°C and 665.5°C are also indicated [5]. Abbreviations; fcc, face centered cubic, hcp, hexagonal close packed, and the rest are described in Figure 18.

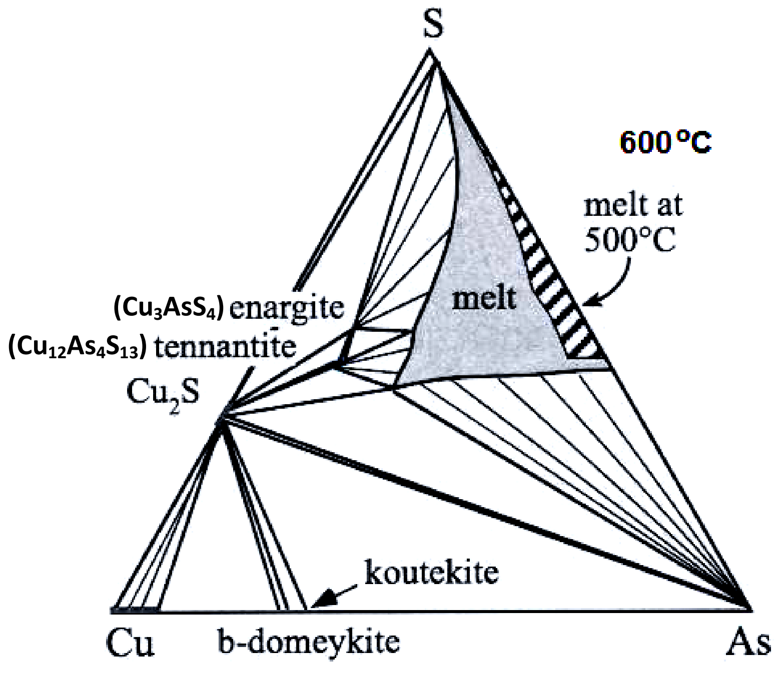

Figure 21. A one bar phase relations in the Cu–As–S system at 600°C and in. Ruled fields show the size of the melt fields in this system at 500°C and one bar; Data from Skinner et al. (1972) and Maske & Skinner (1971) [4].

The first melt in the system Cu–As–S appears on the join As–S, at 281°C. This melt remains Cu-poor until around 500°C, as shown in Figure 18, Figure 19 and Figure 20 . Above 500°C increasing temperature causes the field of liquid to expand to more Cu-rich compositions [4].

3.4 Cu-Sb-S System

Ternary phases in the Cu-Sb-S system are famatinite (Cu_3SbS_4), chalcostibite ($CuSbS_2$), tetrahedrite and a compound labeled as B in Figure 22, Figure 24 and Figure 25 and claimed to be unknown as a mineral, Cu_3SbS_3. The only compound with an extensive composition field is tetrahedrite, for which the composition $Cu_{12+x}Sb_{4+y}S_{13}$ is proposed, where $0 \leq x \leq 1.92$ and $-0.02 \leq y \leq 0.27$. Cu_3SbS_3 was later identified by Karup-Möller et al. [27] among the natural minerals with minor amounts of Ag and named as skinnerite.

The ternary phase relations below 630°C have been extensively investigated by Skinner et al. [9], who presented isotherms at 300, 400, 500, 540 and 600°C (Figure 22). The isotherms at 400 and 600°C detailed by Chang et al. [14] are illustrated in Figure 23. Below T_m (Sb), which 631°C as shown in Figure 5; the phases Cu_3SbS_4, Cu_3SbS_3 and $CuSbS_2$ (chalcostibite) crystallize congruently from the sulfide-rich liquid (L_2) at 627, 607.5 and 553°C, respectively.

All reactions involving the ternary compounds in the system Cu-Sb-S together with the temperatures of reaction as determined in the experimental work of Skinner et al. [9] are listed in Table 9. Few of the reactions may be applied to common mineral assemblages because the natural copper sulfosalts are complex solid solutions in which As and Sb display extensive mutual substitutions and elements such as Fe, Zn and Ag commonly substitute for Cu. They are therefore essential data mainly for completing studies and interpretations in the more complex systems such as Cu-Fe-As-Sb-S. Some of the stable phases in the multi-component systems are discussed in section 3.6.

Table 9. Some reactions in the Cu-Sb-S system. Four pairs of the reactions, which have one or more phases in common, are listed as having the same reaction temperatures, although these reactions theoretically occur at different temperatures, as the breakdown of famatinite [9].

Reaction	Temperature (°C)
Cu_3SbS_3(low T(mon.)) → Cu_3SbS_3 (high T(orth.))	122 ± 3
$CuSbS_2$ + $Cu_{12+x}Sb_{4+y}S_{13}$ + Sb → Cu_3SbS_3	359 ± 2
$Cu_{12+x}Sb_{4+y}S_{13}$ + Sb → Cu_3SbS_3 + fcc	436 ± 2
Cu_3SbS_4 + Sb_2S_3 + S_2 → L	472 ± 2
Cu_3SbS_4 + Sb_2S_3 → $CuSbS_2$ + L	476.5 ± 2
$CuSbS_2$ + Sb_2S_3 → Sb + L	476.5 ± 2
CuS + Cu_3SbS_4 → fcc + liquid sulfur	507± 3
$Cu_{12+x}Sb_{4+y}S_{13}$ + $CuSbS_2$ → Cu_3SbS_4 + Cu_3SbS_3	522± 2
$CuSbS_2$ + Sb → L + Cu_3SbS_3	531± 2
$Cu_{12+x}Sb_{4+y}S_{13}$ → fcc + Cu_3SbS_4 + Cu_3SbS_3	543± 2
$CuSbS_2$ + Cu_3SbS_3 → L + Cu_3SbS_4	543± 2
$CuSbS_2$ + Cu_3SbS_4 → L + liquid sulfur	546.6 ± 2.5
$CuSbS_2$ → L	553 ± 2 (H_m=33.5±0.8 kJ/mol [14])
Sb + Cu_3SbS_3 → L + fcc	588 ± 2.5
Cu_3SbS_4 + Cu_3SbS_3 → L + fcc	588 ± 2
Cu_3SbS_3 → L	607.5 ± 3
fcc + Cu_3SbS_4 → L + liquid sulfur	627 ± 2
Cu_3SbS_4 → L	627 ± 2

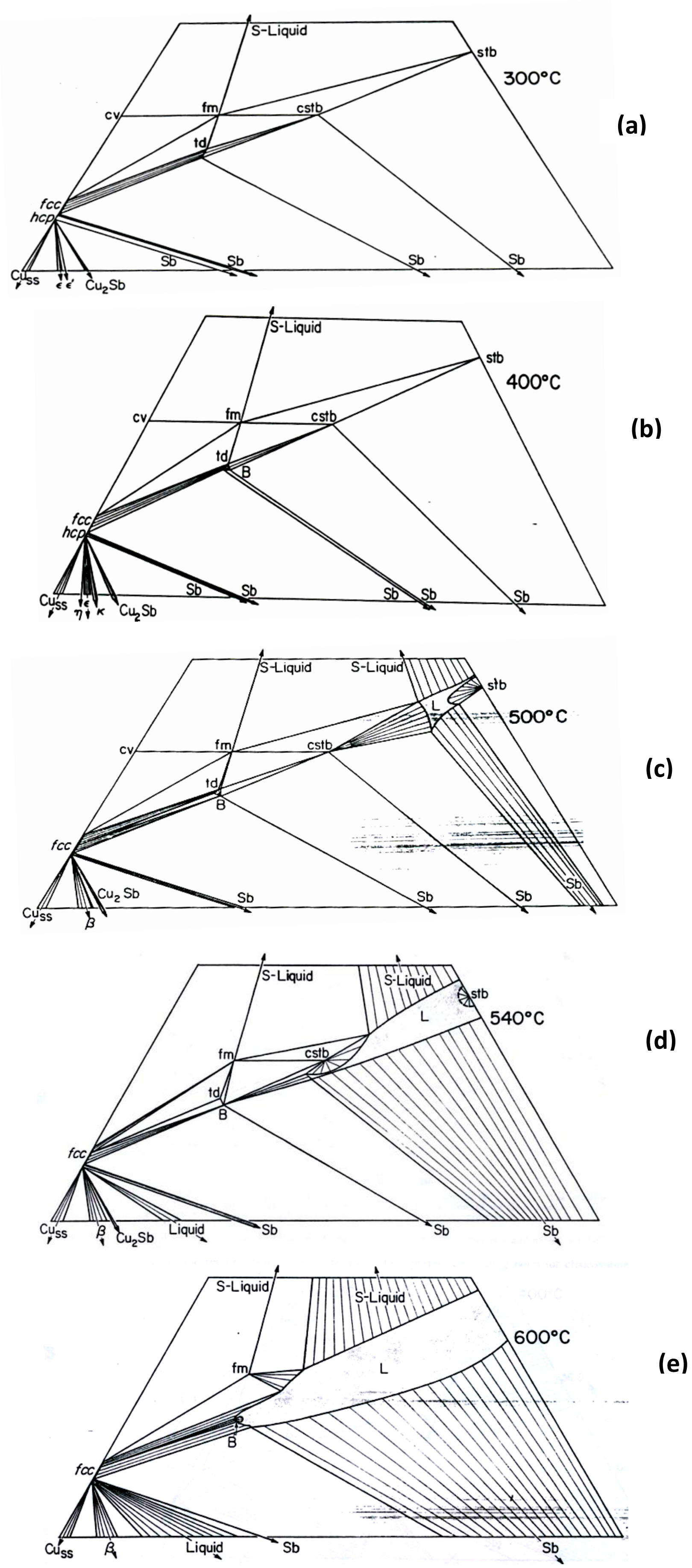

Figure 22.Isothermal phase diagram of the Cu-Sb-S system at (a) 300°C (b) 400°C (c) 500°C (d) 540°C (e) 600°C [9]; the abbreviations are described in Figure 24.

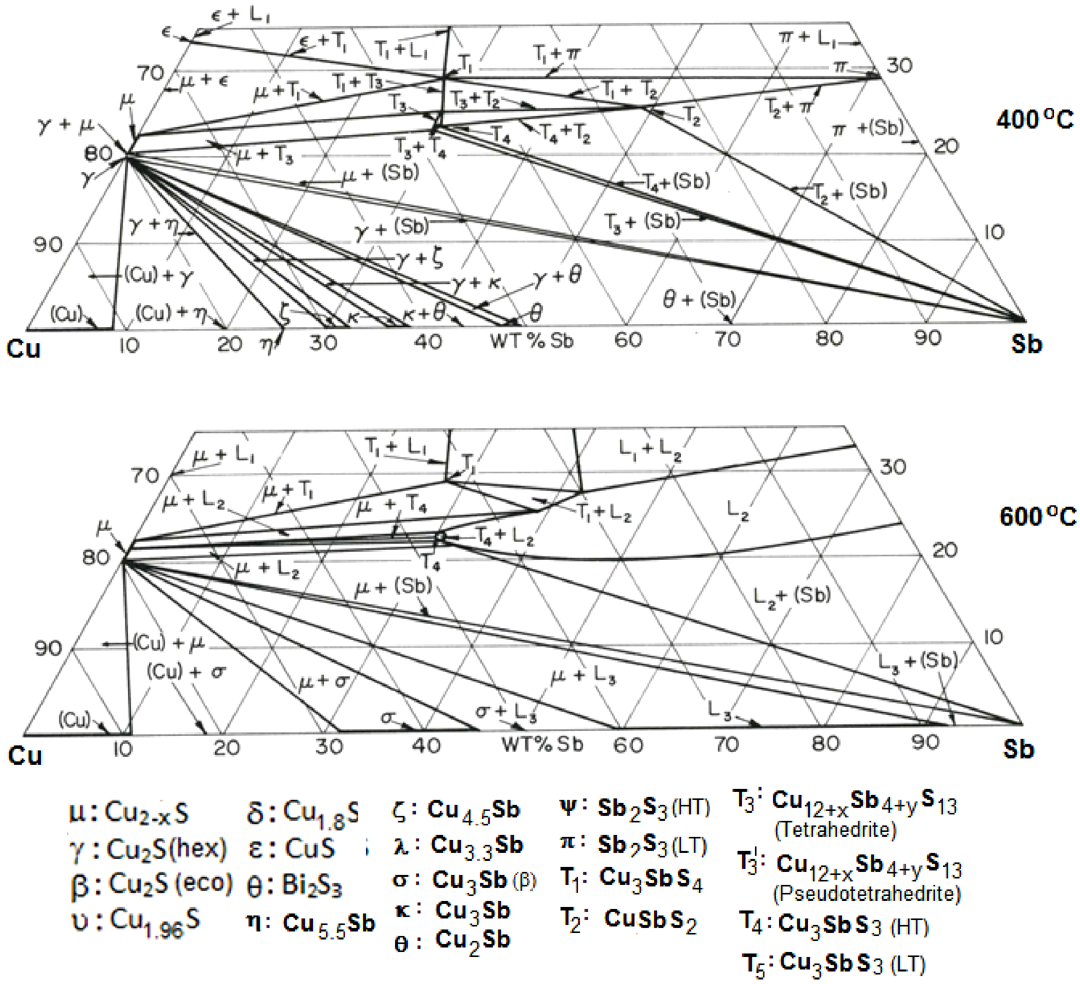

Figure 23. Isothermal section of the Cu-Sb-S system at (a) 400°C and (b) 600°C [14].

The ternary phases of the Cu-Sb-S system can be readily described by an illustration in Figure 24. All of the ternary phases are stable at this temperature (500°C) [9]. Phases in the join between fcc and Sb are stable down to room temperature. The join restricts the stable coexistence of the Cu-Sb alloys with the ternary phases. All of the ternary phases are confined within a narrow composition band bounded by Sb_2S_3, Cu_2S and CuS, and at relatively low temperatures (< 650°C), they all replaced by a liquid that first appears in the ternary near stibnite at 472 ± 2°C, then expands towards chalcostibite and eventually occupies approximately the same band that confines the solid compositions. The sequence of changes involving the various phases in the ternary was determined by completing the isothermal sections shown in Figure 22 [9].

Tetrahedrite is the most common antimonian compound of copper and also appears to be the most common sulfosalt in the earth crust. The mineral is considerably more widespread than its arsenoan isotope tennantite and natural tennantite-tetrahedrite solid solutions tend to be Sb-rich. This unexpected behavior is an artifact of mineral stabilities. In contrast to the tennantite-tetrahedrite case, arsenic forms the common and very stable minerals like arsenopyrite (FeAsS), enargite (Cu_3AsS_4) and löllingite ($FeAs_2$), in which the equivalent antimony compounds are less stable and rare [9].

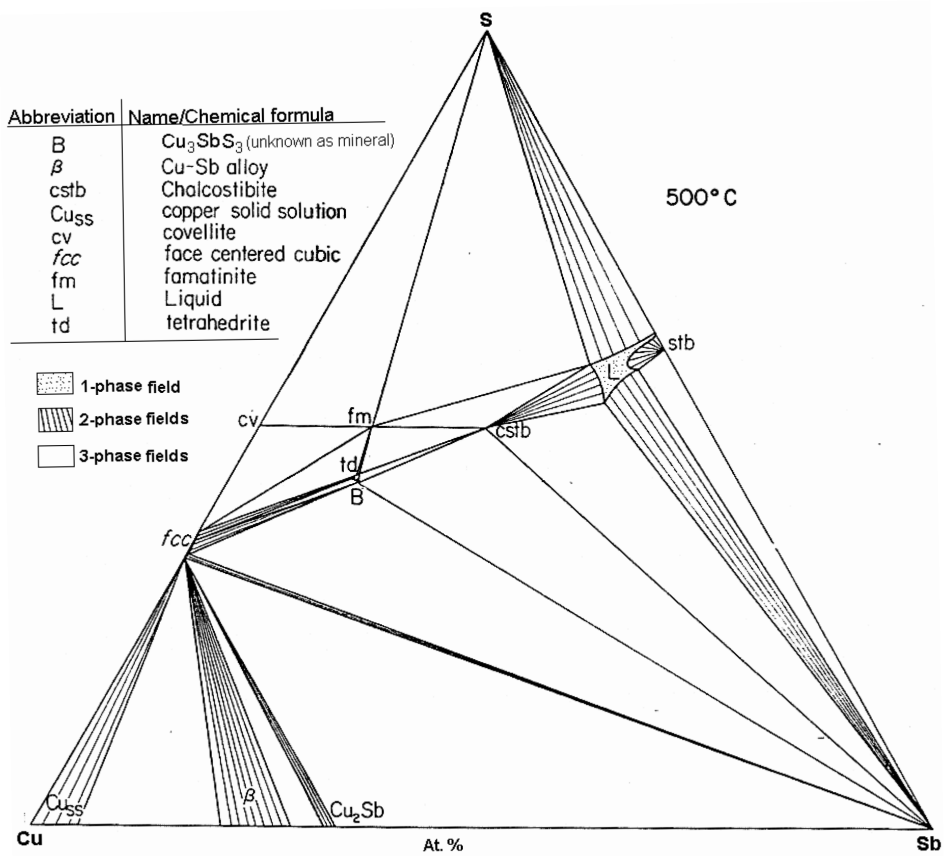

Figure 24. Isothermal section of the Cu-Sb-S system at 500°C [9]; B was later discovered among the natural minerals and named as skinnerite.

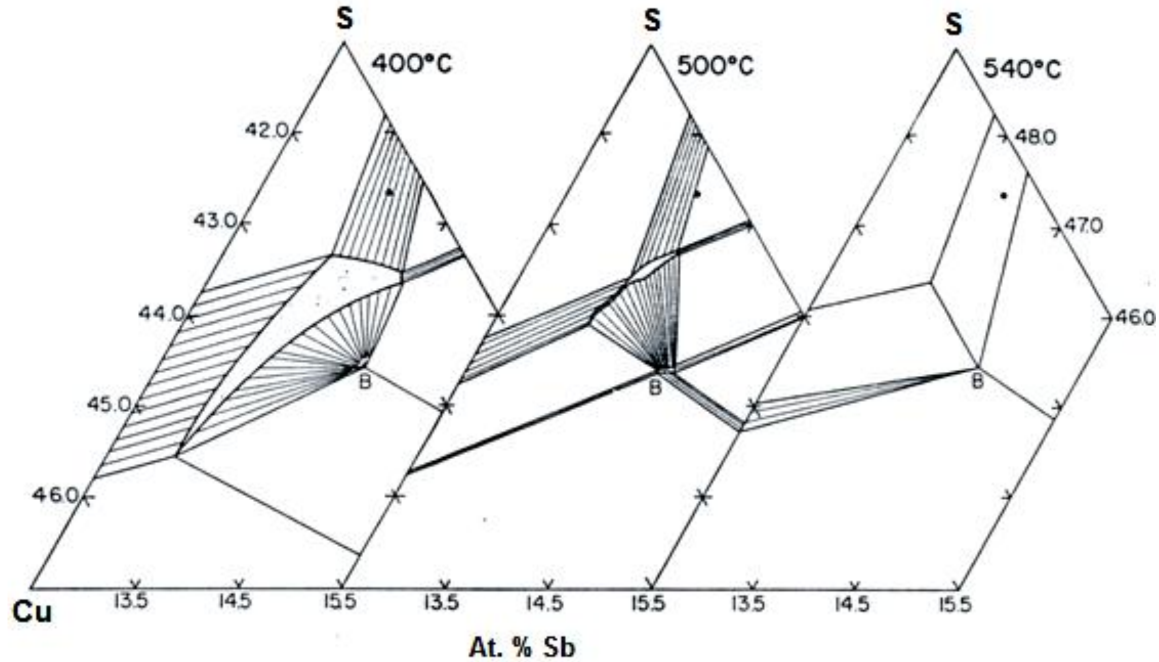

Figure 25. Variation of the tetrahedrite composition field with temperature; the composition $Cu_{12}Sb_4S_{13}$ appears as a solid circle [9].

Based on their experimental studies on the Cu-Sb-As-S system, Skinner et al. [9] concluded that an antimonian tetrahedrite exists in equilibrium with As-rich compounds such as enargite (Cu_3AsS_4) and lautite (CuAsS). Tetrahedrite accommodates several elements such as Zn, Ag, and Hg in solid solution; this will be discussed in section 3.4.

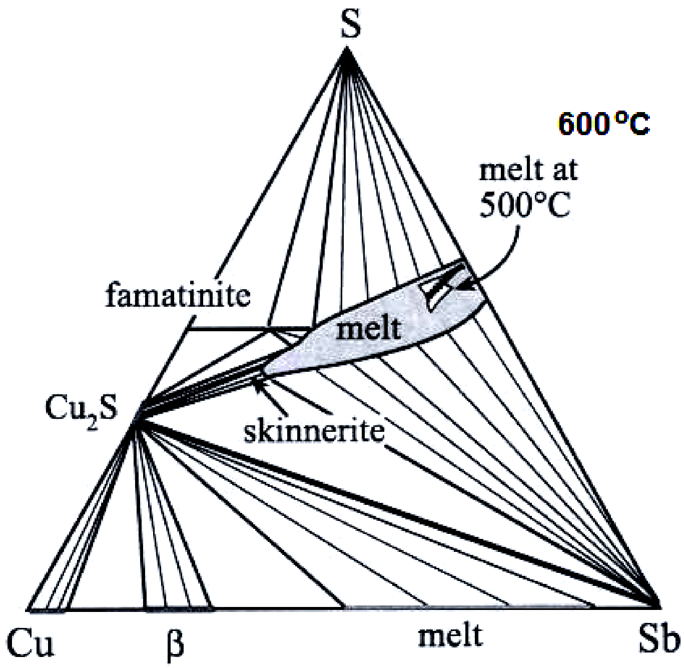

Figure 26. A one bar phase relations in the system Cu–Sb–S at 600°C. Ruled fields show the size of the melt fields in these systems at 500°C and one bar; data from Skinner et al. (1972) and Maske & Skinner (1971) [4].

In the system Cu–Sb–S, the first melts form on the join Sb–S. One melt, which is slightly more S-rich than stibnite (Sb_2S_3), forms at 496°C, whereas another, slightly more Sb-rich than stibnite, develops at 518°C (Skinner et al. 1972) [4]. As in the system Cu–As–S, melt in the system Cu–Sb–S becomes progressively more Cu-rich with increasing temperature, as shown in Figure 26. Tetrahedrite ($Cu_{12+x}Sb_{4+y}S_{13}$, where $0 < x < 1.92$ and $-0.02 < y < 0.27$)) breaks down at 543°C to digenite (Cu_9S_5) + famatinite (Cu_3SbS_4) + skinnerite (Cu_3SbS_3), which is slightly different from the decomposition reaction shown in Table 9. Skinnerite, which has a composition close to that of tetrahedrite, melts at 608°C (Skinner et al. 1972) [4].

Gibbs energies of formation of some sulfosalts and sulfides in the Cu-Sb-S system are summarized in Table 10 and Table 11.

Table 10. Gibbs energy of formation of sulfides and sulfosalts in the Cu-Sb-S system, at 400°C (Standard states: Cu(s), Sb (l) and S_2 (g) at 1atm) [28, 29].

Reaction	ΔG^o(kJ/mol.)	Ref.
$Cu + ½S_2 = Cu_2S$	-110.6 ± 4	Craig and Lees (1972) [28]
$Cu + Sb + \frac{3}{2}S_2 = Cu_3SbS_3$	-273.3	Craig and Lees (1972) [28]
$Cu + Sb + S_2 = CuSbS_2$	-156.5	Craig and Lees (1972) [28]
$Sb + \frac{3}{2}S_2 = Sb_2S_3$	-178.5 ± 2	Craig and Lees (1972) [28]
$2Cu_2S + \frac{4}{3}Sb + S_2 = \frac{4}{3}Cu_3SbS_3$	-143.055	Craig and Lees (1972) [28]
$\frac{2}{3}Cu_3SbS_3 + \frac{4}{3}Sb + S_2 = 2CuSbS_2$	-130.403	Craig and Lees (1972) [28]
$CuSbS_2 + Cu_2S = Cu_3SbS_3$	-1.289	Robert et al. [29]

Table 11. Gibbs energies of formation reactions of some sulfosalts as a function of temperature [30].

Mineral	Reaction	ΔG_f(cal./mol),T(K)	T (°C)	Ref.
$Cu_{12}Sb_4S_{13}$ (Tetrahedrite)	$8Cu_3SbS_3 + S_2=2Cu_{12}Sb_4S_{13}$	-41,572 + 34.84·T	25- 540	Skinner et al. (1972)
Cu_3AsS_4 (Enargite)	$\frac{2}{3}Cu_{12}As_4S_{13} + S_2= \frac{8}{3}Cu_3AsS_4$	-41,576 + 34.91·T	25-500	Wernick & Benson(1957), Maske & Skinner (1971)
Cu_3SbS_4 (Famafinite)	$\frac{2}{3}Cu_{12}Sb_4S_{13} + S_2 = \frac{8}{3}Cu_3SbS_4$	-41,577 + 39.85·T	25- 540	Skinner et al. (1972)
$CuPbSbS_3$ (Bournonite)	$\frac{2}{3}Cu_2S + \frac{4}{3}PbS+ \frac{4}{3}Sb + S_2 = CuPbSbS_3$	-55,684 + 32.96·T	104 - 435	Frumer(1973)
$CuPbAsS_3$ (Seligmannite)	$\frac{2}{3}Cu_2S + \frac{4}{3}PbS+ \frac{4}{3}As + S_2 = CuPbAsS_3$	-46,213 + 32.59·T	104 - 435	Wernick et al. (1958)
$CuPb_{13}Sb_7S_{24}$ (Meneghinite)	$\frac{2}{21}Cu_2S+ \frac{51}{21}Pb+ \frac{4}{3}Sb + S_2 = CuPb_{13}Sb_7S_{24}$	-55,518 +31.89·T	104 - 435	Craig and Barton (1973)

3.4.1 Cu_2S-Sb_2S_3 Quasi-binary System

As shown in Figure 27 the low temperature Cu_2S-rich region is poorly understood. At 622°C, the system is quasi binary only for compositions with $X_{Cu2S} \leq 0.40$ [31]. Using the high temperature reaction calorimetry, Bryndzi and Kleppa [31] studied the enthalpies of formation of chalcostibite ($CuSbS_2$) and monoclinic skinnerite (Cu_3SbS_3), at 298K, from their end-member component sulfides (Cu_2S and Sb_2S_3). They also studied enthalpies of mixing of solid Cu_2S and liquid Sb_2S_3, at 895K, by the solid-liquid reaction calorimetry and expressed the enthalpy of mixing as:

$$\Delta H_{mix}^{S-L} = -9.25 + 18.75X_{Cu_2S} \qquad \text{(at T= 895K for } 0.1 \leq X_{Cu_2S} \leq 0.4) \qquad (15)$$

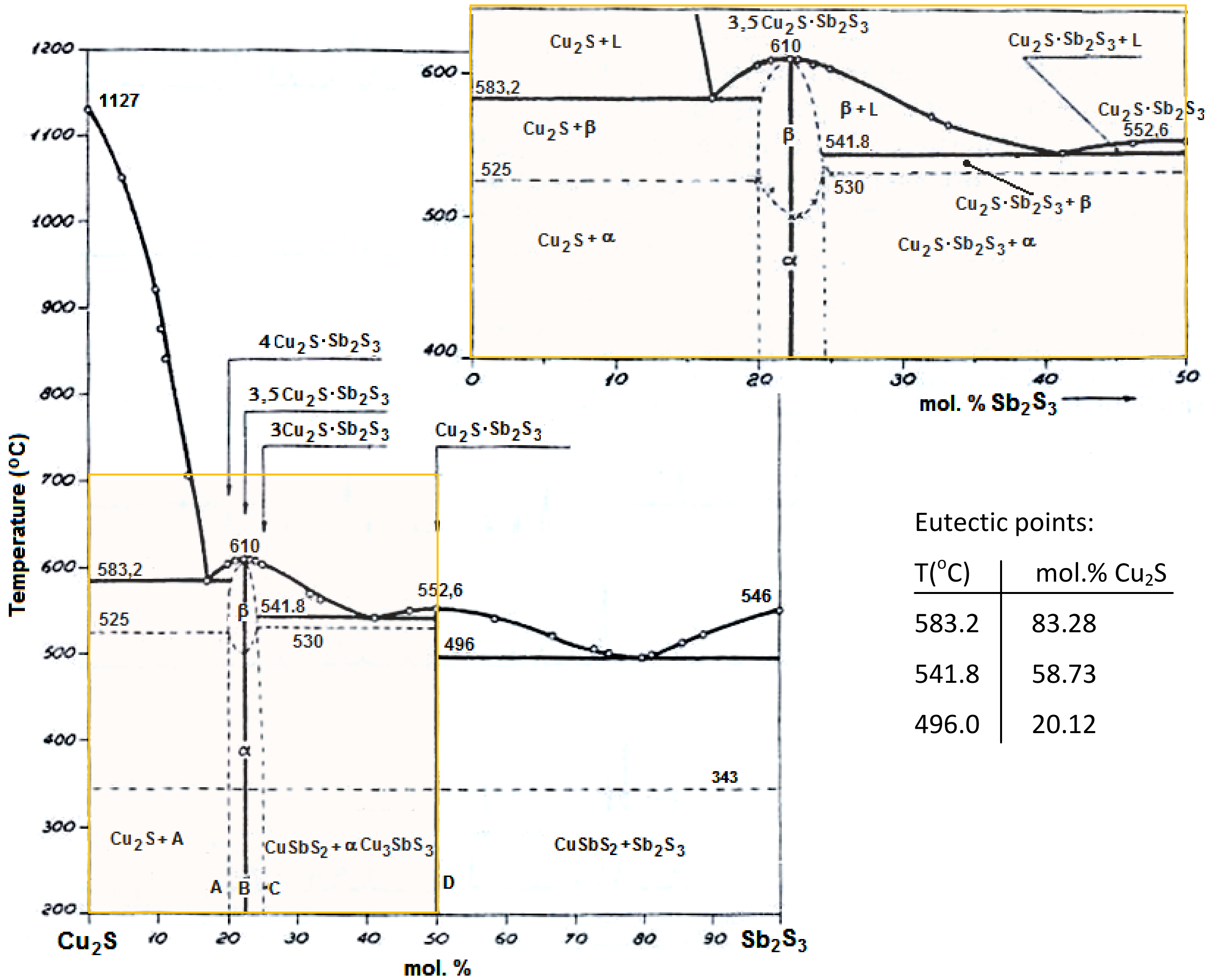

Eutectic points:

T(°C)	mol.% Cu_2S
583.2	83.28
541.8	58.73
496.0	20.12

Figure 27. Phase relations on the Cu_2S-Sb_2S_3 quasi-binary join, taken from Cambi and Elli [32] (modified); A, $4Cu_2S{\cdot}Sb_2S_3$, B, $3.5Cu_2S{\cdot}Sb_2S_3$, C, $3Cu_2S{\cdot}Sb_2S_3$, D, $Cu_2S{\cdot}Sb_2S_3$.

By determining the heat of formation of both sulfosalts at 298K and assuming it does not significantly change up to 673K, Bryndzi and Kleppa [31] summarized the thermochemical data of the two sulfosalts as shown in Table 12.

Table 12. Thermochemical data for $CuSbS_2$ and Cu_3SbS_3 from their component sulfides (Cu_2S and Sb_2S_3) [31].

T(°C)	ΔG_f *(kJ/mol.)	ΔH_f ** (KJ/mol.)	ΔS_f (J/mol.K)
$CuSbS_2$ (chalcostibite)			
25 (orthorhombic)	-17.10	-20.2 ± 2.1	-10.4 ± 3.1 (calculated)
400 (orthorhombic)	-13.17	-20.2 ± 2.1	-10.4 ± 3.1
	-11.93++	-20.2 ± 2.1	-12.3 ± 3.1
Cu_3SbS_3 (skinnerite)			
25 (orthorhombic)	-21.88	-24.8 ± 2.7	9.8 ± 4.0 (calculated)
400 (monoclinic)	-18.20	-24.8 ± 2.7	9.8 ± 4.0
	-18.25++	-24.8 ± 2.7	9.7 ± 4.0

* Values from Verduch and Wagner (1957), and Craig and Lees (1972)
** Experimental results
++ Recalculated from Craig and Lees (1972)

3.5 Cu-(As, Sb)-S System

The compound $Cu(As,Sb)S_4$ occurs in nature with two different crystal structures: orthorhombic Cu_3AsS_4, enargite, tetragonal Cu_3AsS_4, luzonite and tetragonal, Cu_3SbS_4, famatinite. The latter is often referred to as stibio-luzonite in the more recent literature. The stability of an orthorhombic form of Cu_3SbS_4 is not certain. Based on X-ray analysis and chemical data, Gains (1957) showed that there exists a complete solid solution between luzonite and famatinite. Skinner's (1969) thermal phase studies of the Cu-(Sb, As)-S system suggested that complete solid solution between fematinite and enargite does not exist [33]. Phase relationships in the system were determined at temperatures between 100 to 400°C, as shown in Figure 28, from results of quenching experiments, X-ray diffraction, and DTA [8].

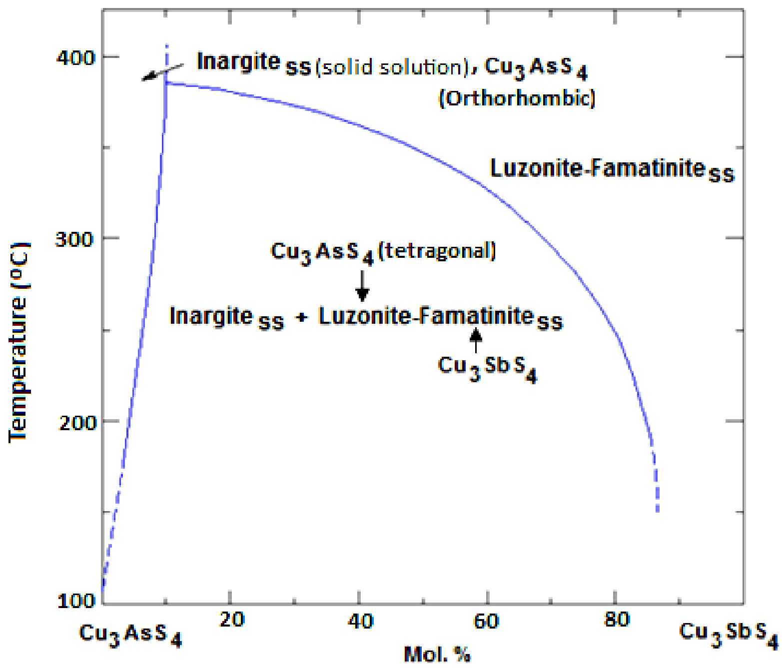

Figure 28. Phase relationships in the Cu_3AsS_4-Cu_3SbS_4 system [8].

In the luzonite-famatinite assemblage, As-Sb substitution takes place widely rather than in enargite-famatinite assemblage. As indicated in Figure 29, enargite may contain up to 6 wt. %Sb (≈20 mol. % famatinite (Cu_3SbS_4)) and Luzonite may contain up to 20 wt. % Sb (≈ 70 mol. % famatinite (Cu_3SbS_4)) [33].

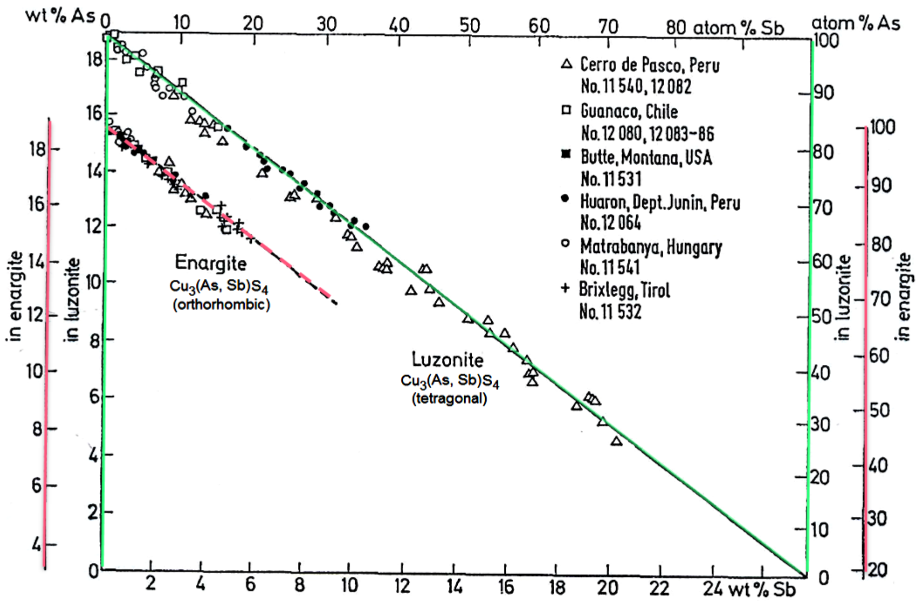

Figure 29. Plot of measured and corrected arsenic versus antimony determinations for luzonite-famatinite (upper(green) curve) and enargite (lower (red) curve); the lines indicate where the measured values should have been if measurements and correction procedures were accurate [33].

3.6 Natural Tetrahedrite and Tennantite in a High Fe and Zn Environments

Owing to different impurities such as Zn, Fe, Ag, Hg, Cd, Co, Au, Mn and others, most natural compositions of tetrahedrite and tennantite are described by the general formula $(Cu, Ag)_{10}(Fe, Zn, Cu, Hg, Cd, Co, Au)_2(Sb, As)_4S_{13}$ [24, 29]. Copper is the leading metal; other metals constitute the isomorphous components. In these natural compositions the ratio Cu(I) : Cu(II) may vary from 10:2 down to 9:3 [24]. Detailed chemical studies of natural mineral samples demonstrated that there exists a limited substitution of Cu, Hg and Cd for Fe and Zn, Bi and Te for Sb and As, and Se for S (Johson et al. 1986) [29]. As mentioned in section 3.5, natural tetrahedrite and tennantite show complex compositions in which As and Sb display extensive mutual substitution, and elements such as Fe, Zn, Hg, and Ag commonly substitute for Cu [35]. For instance, microprobe analysis results of a tetrahedrite sample in Table 13 show the abundant appearance of other elements in the Cu-Sb-S system. As a result of electro-microprobe studies of natural samples of tetrahedrite and tennantite, Robert et al. [29] concluded that Bi and Te are also major impurities, after As and Sb. Thus, the pure Cu-(As, Sb)-S systems discussed in the above sections have a limited applicability to natural systems.

Values of the Gibbs energy of formation can be rigorously calculated from ΔH^o_{298}, S^o_{298}(J/K) and Cp data using the standard equations in chapter 1. Entropies for sulfosalts might be estimated by summing entropies for component sulfides without adjusting for structural differences as in silicates where stronger bonding differences are expected. While studying the Ag-As-S system, Bryndzia & Kleppa [36] noted also that the assumption of no enthalpy of mixing is valid for some sulfosalts.

Table 13. Electron microprobe analyses of tetrahedrite; The results were obtained by using a Camebax-MBX microprobe. Standards were natural and synthetic base-metal sulphides and sulphosalts (standard collection of the Mineralogisches-Petrographisches Institute, University of Heidelberg). ZAF correction was applied [34].

Cu	Sb	S	Zn	Ag	Fe	Total
35.93	23.08	23.18	14.48	2.69	0.83	100.19
33.57	23.38	24.21	11.45	4.89	2.38	99.88
34.58	24.43	23.28	12.56	3.42	1.75	100.02
34.42	24.38	23.65	13.70	3.39	1.59	101.13
34.32	24.42	23.86	13.68	3.67	0.87	100.82
35.80	23.26	22.65	14.06	3.38	1.02	100.47

When considering the "sulfide sum" method, if there exists a similar structure among the component sulfides in the formation of the sulfosalts, the polymorph that is structurally most similar to the sulfosalt should be selected. For example, in approximations for the entropy of Zn-tetrahedrite and Zn-tennantite the entropy value of sphalerite (ZnS) should be used rather than that of wurtzite (ZnS). This is because of the structural similarities between sphalerite and tetrahedrite or tennantite. Likewise, chalcopyrite ($CuFeS_2$) should be selected to model the FeS component in Fe-tetrahedrite and Fe-tennantite. For instance, standard entropy of chalcopyrite itself calculated by this 'sulfide sum' method (124.9 J/mol.K) is only a little bit short of the measured value (126. 8 J/mol.K) reported in the literature [29]. Accordingly, the standard entropies of the sulfosalts, listed in Figure 14, are calculated as follows:

$$S^o_{298,\ Zn\text{-}tennantite} = 5S^o_{298,\ Cu2S} + 2S^o_{298,\ ZnS} + 2S^o_{298,\ As2S3}$$

$$S^o_{298,\ Zn\text{-}tetrahedrite} = 5S^o_{298,\ Cu2S} + 2S^o_{298,\ ZnS} + 2S^o_{298,\ Sb2S3}$$

$$S^o_{298,\ Fe\text{-}tetrahedrite} = S^o_{298,\ Cu2S} - 2S^o_{298,\ CuS} + 2S^o_{298,\ CuFeS2} + 2S^o_{298,\ Sb2S3}$$

$$S^o_{298,\ Fe\text{-}tennantite} = S^o_{298,\ Cu2S} - 2S^o_{298,\ CuS} + 2S^o_{298,\ CuFeS2} + 2S^o_{298,\ As2S3}$$

Based on best fit to available experimental data and natural phase equilibrium constraints expressions for the Gibbs energy of formation for Fe-tetrahedrite ($Cu_{10}Fe_2Sb_4S_{13}$), Zn-tetrahedrite ($Cu_{10}Zn_2Sb_4S_{13}$), Fe-tennantite ($Cu_{10}Fe_2As_4S_{13}$) and Zn-tennantite ($Cu_{10}Zn_2As_4S_{13}$) have been suggested as shown in Table 15. The formation energies of Fe-tetrahedrite from the simple sulfides, at two different temperatures, are also shown in Table 16.

Table 14. Estimated standard thermodynamic variables for Fe-tennantite, Zn-tennantite, Fe-tetrahedrite and Zn-tetrahedrite [29]; molar enthalpies of formation are relative to the elements and S_2(g) at 1 atm.

Phase	ΔH^o_{298}(kJ)	S^o_{298}(J/K)	V_{298}(cm^3)
Fe-tennantite	-1968.6	1048.9	322.1
Zn-tennantite	-2150.0	1048.9	322.1
Fe-tetrahedrite	-1909.5	1085.7	336.7
Zn-tetrahedrite	-2091.9	1085.7	336.7

Table 15. Recommended Gibbs energy of formation for tetrahedrite and tennantite (relative to the elements and ideal gas S_2), Robert et al. (1990) [29].

Phase (mineral name)	ΔG^o(kJ/mol), where T in K	Temperature range (^{o}C)
$Cu_{10}Fe_2As_4S_{13}$ (Fe-tennantite)	-1,933,305 + 865.7·T (-1,610,268 + 819.2·T)*	25 – 602
$Cu_{10}Zn_2As_4S_{13}$ (Zn-tennantite)	-2,119,070 + 908.3·T (-1,847,749 + 895.9·T)*	25 – 420
	-2,130,050 + 923.9·T (-1,847,749 + 895.9·T)*	420 – 602
$Cu_{10}Fe_2Sb_4S_{13}$ (Fe-tetrahedrite)	-1,871,251 + 860.8·T (-1,728,628 + 823.5·T)*	25 – 630
$Cu_{10}Zn_2Sb_4S_{13}$ (Zn-tetrahedrite)	-2,058,151 + 903.2·T (-1,966,109 + 900.0·T)*	25 – 420
	-2,069,130 + 918.9·T (-1,966,109 + 900.0·T)*	420 – 630

* Calculated *by Craig & Barton approximation methods (Relative to simple sulfides such as: Cu_2S, FeS, ZnS, Sb_2S_3, As_2S_3):* $\Delta G^o(sulfosalt) = \sum_1^n \Delta G_i^o(sulfide)$, *an approach which assumes H_M = 0, but uses a theoretically derived term for entropy of mixing.*

Table 16. Formation of energies of $Cu_{10}Fe_2Sb_4S_{13}$ from simple sulfides at 1 bar and standard state free energy of Fe-Zn exchange reaction; standard states: Cu_2S(S), FeS(S) and Sb_2S_3(S) [37].

Reaction	T(^{o}C)	H_f(kJ/gfw)	S_f(kJ/K.gfw)	ΔG_f(kJ/gfw)
$Cu_2S + FeS + Sb_2S_3 = Cu_{10}Fe_2Sb_4S_{13}$	200	-	-	-63.92
	400	-35.9964	59.02	-75.73
$½Cu_{10}Fe_2Sb_4S_{13} + ZnS = FeS + ½Cu_{10}Zn_2Sb_4S_{13}$	25	-	-	8.6684

Table 17. Heat capacities for Fe-tennantite, Zn-tennantite, Fe-tetrahedrite and Zn-tetrahedrite [29]; estimated by summing the expressions of the component sulfides in the stoichiometric proportions of the sulfosalts.

Phase	Heat capacity coefficients ($Cp = a + b\cdot T + c\cdot T^{-2} + d\cdot T^{-0.5}$)			
	a	$b\cdot 10^3$	$c\cdot 10^{-4}$	d
Fe-tennantite	- 627.3	792.20	-2944.1	25499.4
Zn-tennantite	734.9	83.43	-97.1	-
Fe-tetrahedrite	-634.5	840.40	-2944.1	25499.4
Zn-tetrahedrite	727.3	131.63	- 97.1	-

3.6.1 Equilibrium Reactions and Phase Assemblages

At higher fS_2 values, tennantite stability is restricted by reactions involving enargite (Cu_3AsS_4), or its low-temperature polymorph, luzonite. The assemblages reported in the literature suggest that these phases are related within the chalcopyrite field through the reaction:

$$4Cu_3AsS_4 + 4FeS_2 = Cu_{10}Fe_2As_4S_{13} + 2CuFeS_2 + 7/2S_2 \quad (16)$$

Due to lack of thermodynamic data for enargite and luzonite, this reaction is only schematically represented in Figure 30, based on the assemblage presented in the literature [29].

Fe-tetrahedrite stability is also restricted by the reaction:

$$Cu_{10}Fe_2Sb_4S_{13} + 2FeSb_2S_4 + 11/2S_2 = 10CuFeS_2 + 4Sb_2S_3 \quad (17)$$

These equilibria greatly restrict the stability of the assemblage chalcopyrite ($CuFeS_2$) + stibnite (Sb_2S_3). Given that tetrahedrite is the only phase that exhibits appreciable solid-solution, any solid-solution substitution would shift the location of these reactions so as to eliminate the stability of chalcopyrite + stibnite in most natural setting.

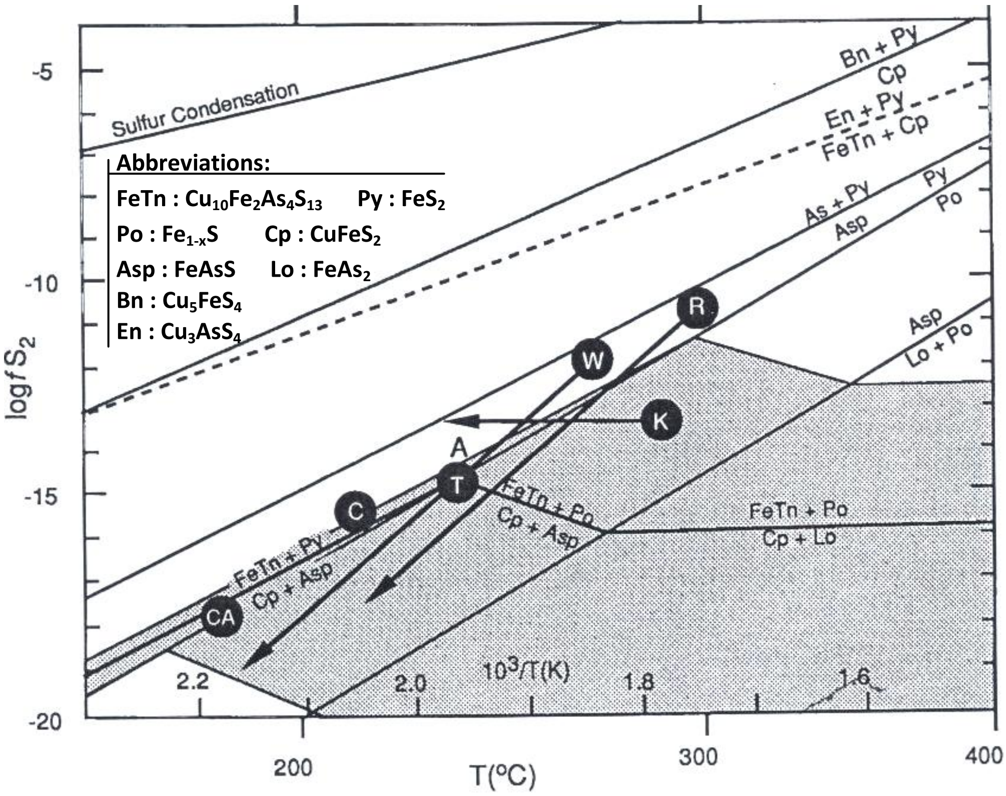

Figure 30. Phase equilibria in the Cu-Fe-As-S system as a function of temperature and sulfur fugacity; dashed curve represent schematically depicted equilibria. Symbols: R Ramshorn mine, C Clayton Silver mine, W Woodlawn mine, K Keno Hill, T Topia district, and CA Coeur d'Alene district. Arrows represent general trends recorded by the assemblages from these areas. The shaded area represents the uncertainty in the equilibria relating Fe-tennantite to arsenopyrite (Asp) or löillingite (Lo) resulting from reported precision of the $\Delta H^o_{f,298}$ value. Thermodynamic data for sulfides from Barton & Skinner (1979) [29].

The formation of skinnerite (Cu_3SbS_3) is limited by Zn and Fe deficient environments and restricted by Zn and Fe-tetrahedrite environments. In skinnerite-bearing assemblages the stability of Zn-tetrahedrite is limited by the reactions:

$$3Cu_{10}Zn_2Sb_4S_{13} = 10Cu_3SbS_3 + 2Sb + 6ZnS + 3/2S_2 \quad (18)$$

$$3Cu_{10}Zn_2Sb_4S_{13} = 10Cu_3SbS_3 + Sb_2S_3 + 6ZnS \quad (19)$$

and

$$Cu_{10}Zn_2Sb_4S_{13} = 5Cu_2S + 4Sb + 2ZnS + 3S_2 \quad (20)$$

Conversely, the stability of skinnerite, which is incompatible with sphalerite (exists only at a very low a_{ZnS}), is constrained by the reactions:

$$2Cu_3SbS_3 = 3Cu_2S + 2Sb + 3/2S_2 \quad (21)$$

and

$$4Cu_3SbS_3 + 2ZnS = Cu_{10}Zn_2Sb_4S_{13} + Cu_2S \quad (22)$$

According to the above reactions the sphalerite-bearing assemblages lack skinnerite, as it would be expected for environments with a_{ZnS} values sufficiently high to stabilize sphalerite [29].

3.7 Cu-Bi-S System

Phase equilibria in this system are mainly studied along the join Cu_2S-Bi_2S_3. On this join several ternary phases such as Cu_9BiS_6, $CuBi_3S_5$, $Cu_3Bi_5S_9$, $Cu_{24}Bi_{26}S_{51}$, $CuBiS_2$, Cu_3BiS_3 and Cu_9BiS_6 are reported. The high temperature relations, on the join, can be seen in Figure 31.

Table 18. Estimated four-phase equilibria in the Cu-Bi-S system [14].

Reaction	Temperature(°C)
$L_{sulfide-rich} + Cu_{2-x}S = L_{metal-rich} + Cu_2S$	< 645
$L_{sulfide-rich} + Cu_2S = L_{metal-rich} + Cu_3BiS_3$	< 517
$L_{sulfide-rich} = L_{metal-rich} + Cu_3BiS_3 + Cu_{3+x}Bi_{5-x}S_9$	< 512
$L_{sulfide-rich} + Cu_{3+x}Bi_{5-x}S_9 = L_{metal-rich} + CuBi_3S_5$	< 588
$L_{sulfide-rich} + Bi_2S_3 = L_{metal-rich} + CuBi_3S_5$	< 645

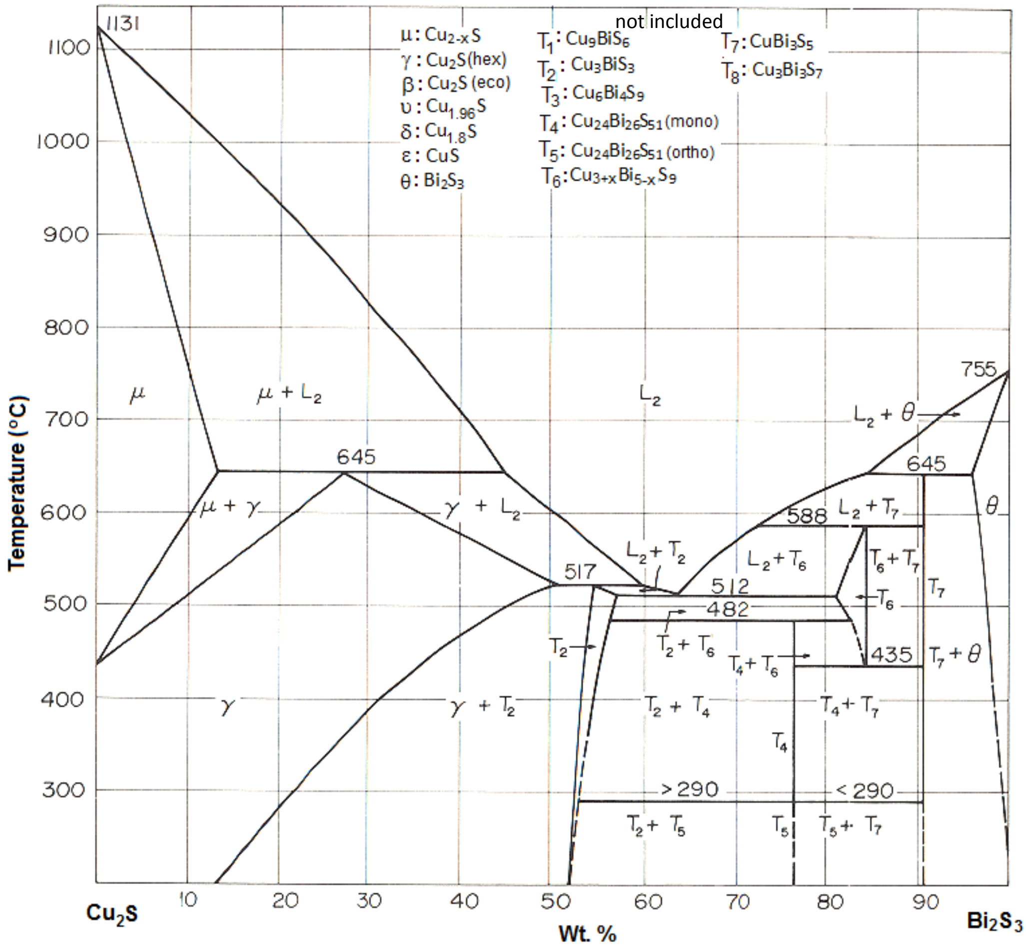

Figure 31. The Cu_2S-Bi_2S_3 pseudo-binary phase diagram [14]; an estimate for the four phase-equilibria is shown in Table 18.

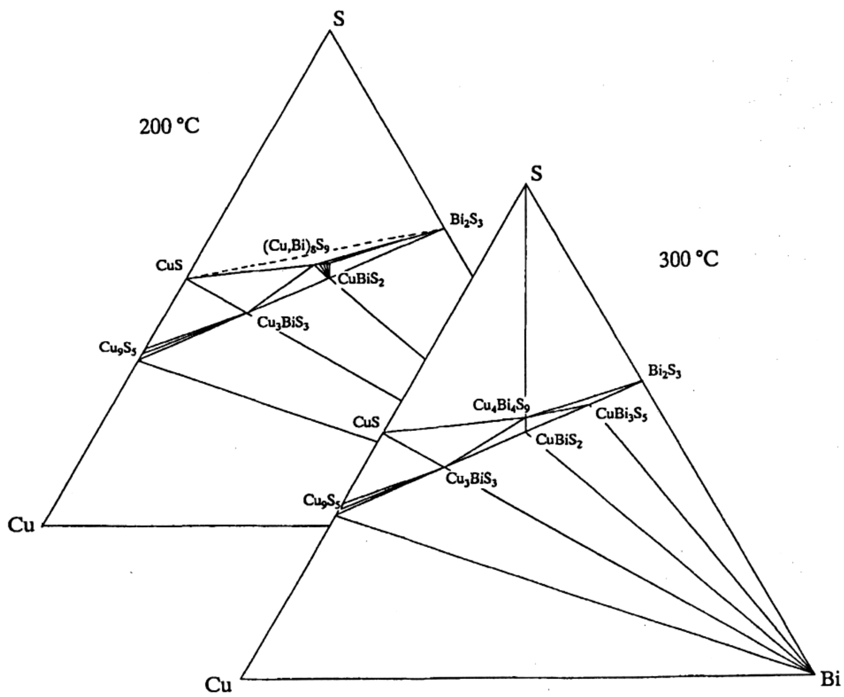

Figure 32. Isothermal section of the Cu-Bi-S system at 200°C and 300°C [38].

According to Wang [38] at 200°C, two ternary phases are stable on the Cu_2S-Bi_2S_3 join; Cu_3BiS_3 (wittichenite) and $CuBiS_2$ (emplectite). Both of them, as well as Cu_2S or its Bi-bearing members, coexist with metallic bismuth. He also reported that primary sulfidation at 178°C produced metastable series $Cu_{10}Bi_2S_{13}$-$Cu_5Bi_2S_8$ on the CuS-Bi_2S_3 join, and coexist with CuS. However, its Bi-rich partial range was found to break down after extended heating at 200°C whereas the Cu-rich partial range remains unaltered. Consequently, all phase assemblages which involve this series were considered to be metastable and excluded from the 200°C isotherm shown in Figure 32. A second solid-solution series, intermediate to the two joins, $(Cu, Bi)_8S_9$, coexists stably, at 200°C with Cu_3BiS_3, $CuBiS_2$ and Bi_2S_3. Because of uncertainties observation on the CuS-Bi_2S_3 join the tie line is plotted as a dashed line on the 200°C isotherm. At 300°C the phases Cu_3BiS_3 and $CuBiS_2$ persist on the Cu_2S-Bi_2S_3 join. The $(Cu,Bi)_8S_9$ series becomes slightly metal-enriched with compositions approaching $Cu_4Bi_4S_9$. Tie lines radiates from this phase to six phases: CuS, Cu_3BiS_3, $CuBiS_2$, $CuBi_3S_5$, Bi_2S_3 and sulfur (Figure 32).

Sulfidation experiments on Cu_3BiS_3 similarly revealed a solid solution range for the phase $(Cu,Bi)_8S_9$ where Cu/Bi = 3/2 at 178 -190°C, and a lower stability limit of 138°C [38]. This S-rich ternary phase $Cu_4Bi_4S_9$, shown in Figure 32, is obtained through the reactions (23) and (24).

$$2CuS + Cu_2S + 2Bi_2S_3 \rightarrow Cu_4Bi_4S_9 \qquad (T=300^oC) \qquad (23)$$

$$CuBiS_2 + S_2 \rightarrow Cu_4Bi_4S_9 \qquad (T=300^oC) \qquad (24)$$

$$Cu_3BiS_3 + S_2 \rightarrow Cu_4Bi_4S_9 + CuS \qquad (T=138^oC) \qquad (25)$$

Detailed synthesis over the temperature range 120 – 500°C revealed that at 300°C and lower temperatures, $Cu_4Bi_4S_9$ and S-rich members are stable. With increasing temperature, the phase $(Cu,Bi)_8S_9$ become metal enriched with in the stoichiometric 8/9 formula.

The assemblage $Cu_4Bi_4S_9$-Bi_2S_3 is stable up to 420°C after which it transforms into the assemblage $CuBi_3S_5$ss + L_{sulfur}. $CuBi_3S_5$ exists in a various assemblages only above 275°C. The phases cuprobismutite ($Cu_{10}Bi_{12}S_{23}$) and $Cu_3Bi_5S_9$, on the Cu_2S-Bi_2S_3 join, appear also at higher temperatures [38].

As illustrated in Figure 33 $CuBiS_2$ (cuprobismuthite) forms a binary solid solution with $CuBi_3S_5$. It melts at about 469.2°C [39], and exists over a range between 52 and 47% Cu_2S at 454°C (Figure 33) and between 51 and 48 %Cu_2S at 300°C [8]. In the presence of Ag_2S, Cu_3BiS_3 forms a solid solution $(Cu_{0.08}Ag_{0.2})_3BiS_3$ at 454°C. A complete solid solution exists between $CuBi_3S_5$ and $AgBi_3S_5$ with a large area of ternary solid solution near the $CuBi_3S_5$-end [8]. However, a study by Daqing [40], as shown in Figure 34, showed that there is no complete solid solution between the phases. He rather reported a maximum of 9 mol. % Ag_2S in $Cu_3Bi_5S_9$ss which extends towards $AgBi_3S_5$ss.

Unpublished work of Skinner and Makovicky has shown that at 375°C Sb substitution for Bi in Cu_3BiS_3 may exceed 50 %, but the solubility of Bi in Cu_3SbS_3 at the same temperature is only less than 10 % [27]; suggesting that at the presence of excess Sb, mineral assemblages in the Cu-Bi-Sb-S system are richer in phases of the Cu-Sb-S system.

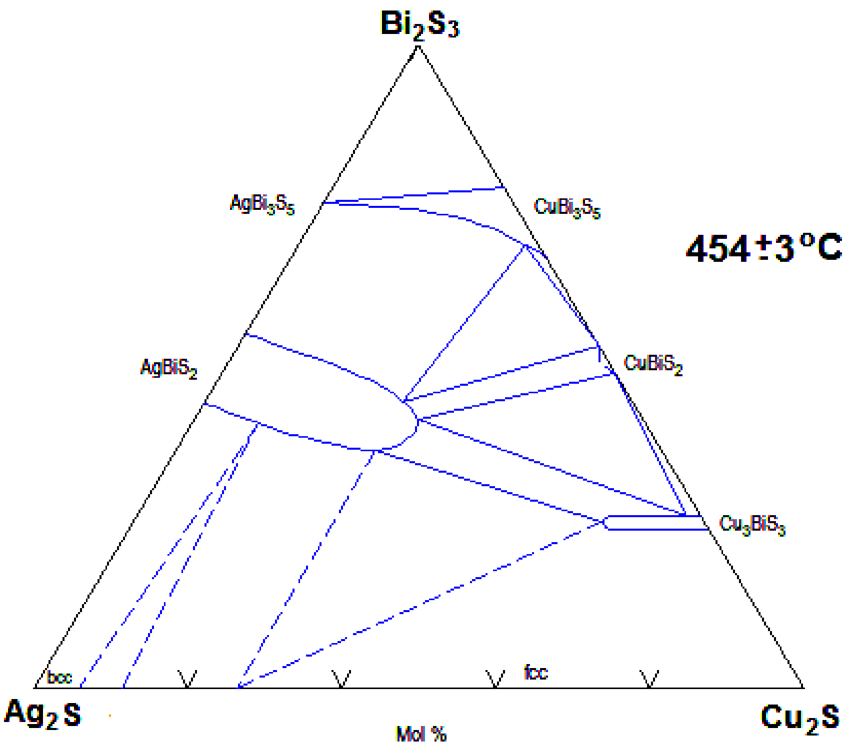

Figure 33. Isothermal section of the Ag_2S-Cu_2S-Bi_2S_3 system at 454°C [8].

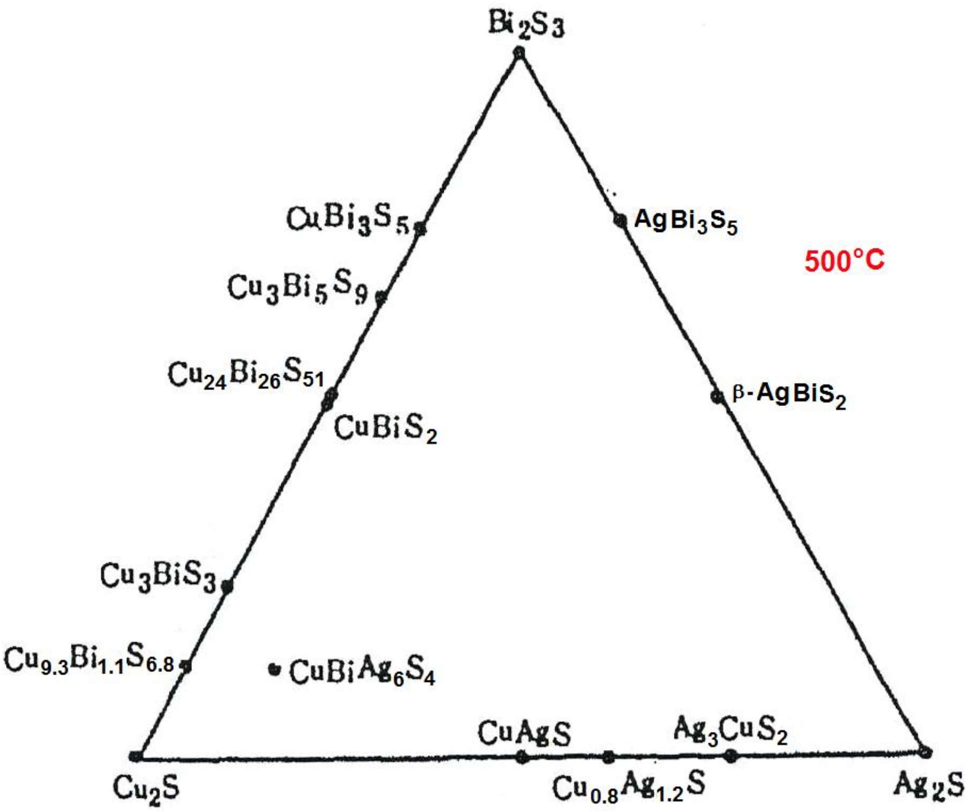

Figure 34. Isothermal section of the Ag_2S-Cu_2S-Bi_2S_3 system at 500°C [40].

The intermediate phases in the Cu_2S-Bi_2S_3 system at 500°C include Cu_9BiS_6, $CuBi_3S_5$, $Cu_3Bi_5S_9$, $Cu_{24}Bi_{26}S_{51}$, $CuBiS_2$, Cu_3BiS_3 and Cu_9BiS_6 [40], all but Cu_9BiS_6 are shown in Figure 34. Cu_9BiS_6, which exists in the high temperature Cu_2S-rich portion, as reported from volcanic lavas in Argentina has a cubic structure and very similar to the 'unidentified' mineral $Cu_{9.3}Bi_{1.1}S_{6.8}$. The $Cu_3Bi_5S_9$ compound is stable above 442°C and experimental works showed that there exists solid solution around its stoichiometric composition. Cuprobismutite, $Cu_{24}Bi_{26}S_{51}$, is stable between 474 ± 5°C – 319 ± 2°C [40].

The Gibbs energies of formation of the ternary phases, via different reaction routs, are summarized in Table 19 and Table 20.

Table 19. Gibbs energies of formation reactions from the elements, binary and ternary sulfides at 510°C (standard states: Cu(s), Bi (l) and S_2 (g) at 1atm) [14, 28].

Reaction(A)	ΔG_r(kJ/mol) reaction (A)	Reaction (B) (S_2(g) @1atm.)	ΔG_f(kJ/mol) reaction (B)
$6Cu_2S + \frac{4}{3}Bi + S_2 = 2Cu_9BiS_6$	-108.5	$9Cu + Bi + 3S_2 = Cu_9BiS_6$	-567.08
$\frac{2}{3}Cu_9BiS_6 + \frac{4}{3}Bi + S_2 = 2Cu_3BiS_3$	-94.02	$3Cu + Bi + \frac{3}{2}S_2 = Cu_3BiS_3$	-238.05
$\frac{1}{3}Cu_3BiS_3 + \frac{4}{3}Bi + S_2 = \frac{1}{3}Cu_3Bi_5S_9$	-90.25	$3Cu + 5Bi + \frac{9}{2}S_2 = Cu_3Bi_5S_9$	-521.07
$\frac{1}{3}Cu_3Bi_5S_9 + \frac{4}{3}Bi + S_2 = CuBi_3S_5$	-88.94	$Cu + 3Bi + \frac{5}{2}S_2 = CuBi_3S_5$	-266.67

Based on the Gibbs energies of formation of Cu_2S and Bi_2S_3, Chang's [14] calculation for the Gibbs energies of formation of the ternary phases is reorganized as shown in Table 20. The stability ranges of all the binary and ternary phases in Table 19 and Table 20 are shown in Figure 31.

Table 20. Gibbs energies of formation of Cu_2S and Bi_2S_3 and ternary phases as a result of their reactions at 510°C (Standard states: Cu(s), Bi (l) and S_2 (g) at 1atm).

Composition	$X_{Bi_2S_3}$	ΔG_f(kJ/mol of Cu_2S and Bi_2S_3)
$2Cu + \frac{1}{2}S_2 = Cu_2S$	0.000	-107.2 ± 4
$\frac{3}{2}Cu_2S + \frac{1}{2}Bi_2S_3 = Cu_3BiS_3$	0.250	-4.4
$\frac{3}{2}Cu_2S + \frac{5}{2}Bi_2S_3 = Cu_3Bi_5S_9$	0.625	-4.6
$\frac{1}{2}Cu_2S + \frac{3}{2}Bi_2S_3 = CuBi_3S_5$	0.750	-3.9
$2Bi + \frac{3}{2}S_2 = Bi_2S_3$	1.000	-136.8 ± 4

3.8 Zn-As-S System

Contrary to Ni and Cu, Zn melts and boils at relatively low temperatures of 419°C and 927°C, respectively [41]. The phase relations in the binary Zn-As system are shown in Figure 35.

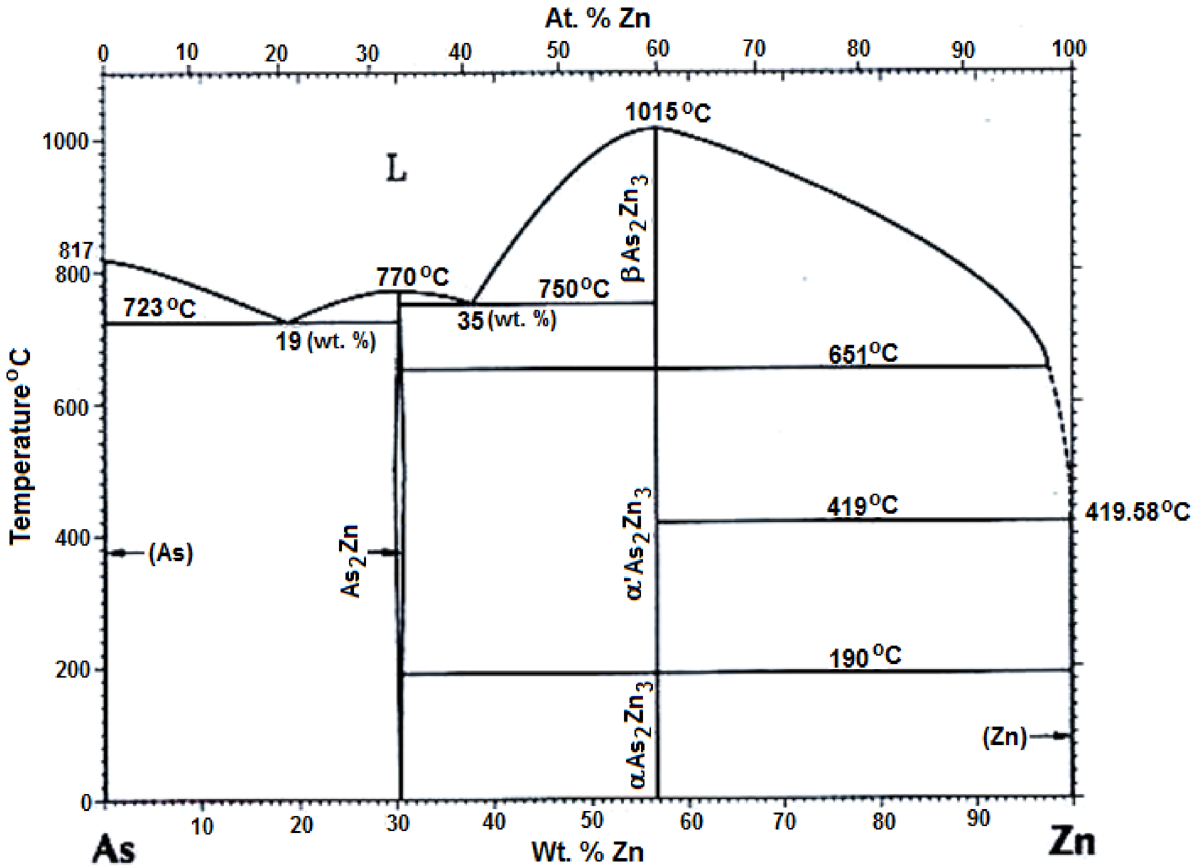

Figure 35. The Zn-As phase diagram (H. Okamoto, 1992) [17].

Studies on the broader Zn-As-S system are very limited. The only study on this system, by Olekseyuk and Tovtin [42], showed that synthesis of alloys along the ZnS-As_2S_5 join to not result in any ternary phase; however, they couldn't equilibrate any phase on the join line. In their investigations into the nature of the physicochemical interactions in the Zn_3As_2-ZnS, As-ZnS, As_2S_2-ZnS and As_2S_3-ZnS sections below 1100°C, they also encountered no ternary phase.

The Zn_3As_2-ZnS phase diagram, shown in Figure 36, is peritectic at 10.5 mol. %ZnS. The solubility of ZnS in β-Zn_3As_2 at the peritectic temperature is ~16 mol. % ZnS and falling to 7 mol. % ZnS at 610°C and to 1 mol. % ZnS at 240°C. The equilibrium diagrams of the $ZnAs_2$-ZnS, As-ZnS, As_2S_2-ZnS and As_2S_3-ZnS sections are eutectic at 0.5, 0.7, 0.9 and 3 mol. % ZnS and at 761.85, 785.85, 301.85 and 299.85°C, respectively.

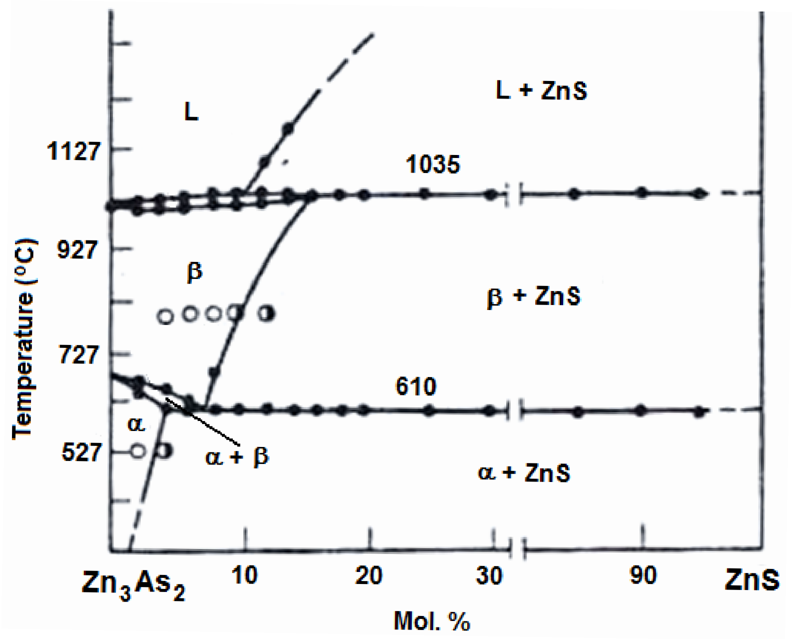

Figure 36. Phase diagram of the pseudo-binary Zn_3As_2-ZnS system [42].

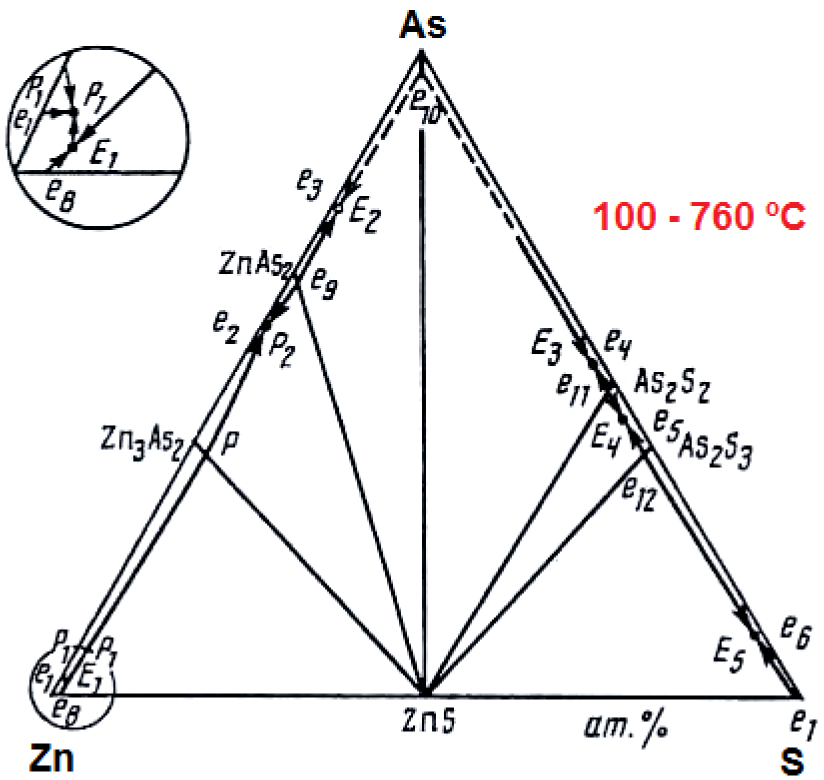

Figure 37. Liquidus surface of the Zn-As-S system [42]; E_i represents ternary eutectics and P_i represents peritectic points.

Generally, there are nine phase crystallization fields in the Zn-As-S system: ZnS, β-solid solutions based on Zn_3As_2, α-solid solutions based on Zn_3As_2, $ZnAs_2$, As, As_2S_2, As_2S_3, S and Zn. These fields are separated by 15 curves of univariant equilibria. The seven invariant equilibria points observed are listed in Table 21. At 226.85^{o}C a homogenous single phase region to exist only around the Zn_3As_2 corner, as shown in Figure 37 [42].

Table 21. Invariant processes which take place in the Zn-As-S system [42].

Notations in Figure 37	Reaction	Temperature(^{o}C)
E_1	L ⇌ZnS+ β-Zn_3As_2 + Zn	416.85
E_2	L ⇌ ZnS + $ZnAs_2$ + As	664.85
E_3	L ⇌ ZnS + As_2S_2 + As	289.85
E_4	L ⇌ ZnS + As_2S_2 + As_2S_3	274.85
E_5	L ⇌ ZnS + As_2S_3 + S	~99.85
p_1	L + β-Zn_3As_2⇌ α-Zn_3As_2 + Zn	417.85
p_1	L + ZnS ⇌ β-Zn_3As_2 ZnAs2	759.85

4 Summary and Conclusions

Phase equilibria in the As-S, Sb-S and Bi-S systems are reviewed. The Cu-based systems are relatively intensively studied. Several stable phases and their stability ranges have been reported by different researchers. Sulfosalts of this system, tetrahedrite and tennantite, are the most stable relative to other sulfosalts and certain other sulfide phases. Thus, it is this stability that accounts for their common occurrence in a variety of mineral ore deposits.

Experimental studies below 700^{o}C showed that the Ni-As-S system comprises a single stoichiometric stable ternary phase called gersdorffite (NiAsS). This ternary phase exhibits extensive solid solutions of arsenic and sulfur. Stable phases in the Ni-Sb-S system resemble that of stable phases in the Ni-As-S system. In this system also, only one stoichiometric ternary phase, namely ullmennite (NiSbS) has been reported to be stable. In this system substitutions of Co for Ni and As for Sb are major mechanisms of solid solution formations. Thermodynamic properties and phase equilibria of the Zn-As-S system are rare among published works. A study about this system, below 760^{o}C, has shown that there is no ternary phase stable.

In general, the ternary systems have complex phase-relations, which may be as a result of the very low differences in their Gibbs energies of formation. Thermodynamic data for most ternary phases are limited to a certain temperature range (350 ± 200^{o}C) only. However, despite the fact that the Gibbs energies of formation of the sulfosalts are so close to each other, it may be possible to determine the formation energies of some sulfosalts computationally.

Acknowledgements

The authors are grateful to Improved Sulfide Smelting (ISS) project of the ELEMET program and Tekes, the Finnish Funding Agency for Technology and Innovation, for financial support. This work was made as a sub task of ISS, supported financially by Boliden Harjavalta Oy, Boliden Kokkola Oy, Norilsk Nickel Finland Oy and Outotec Oyj.

5 References

1. Tesfaye Firdu, F. & Taskinen, P. Sulfide Mineralogy - Literature Review. Aalto University Publications in Materials Science and Engineering, Thermodynamics and Modeling of Metallurgical Processes. Espoo. TKK-MT-214, ISSN 1455-2329. 2010. 48 p. ISBN 978-952-60-3271-9

2. Hietanen, P. Epäpuhtaussulfidisysteemien tasapainot ja termodynamiikka sekä Ag-Te-systeemin tutkiminen emf-tekniikalla. Diplomityö. Aalto-yliopiston teknillinen korkeakoulu, Materiaalitekniikan tutkinto-ohjelma. Espoo. 2010. s. 66.

3. Taskinen, P. Tasapainopiirrosten optimointi ja laskenta. Seminaari Lukas-ohjelmisto käytöstä. TKK, Mvt-laboratorio, Otaniemi. Report TKK-V-C95. 1989. s. 22.

4. Ronald Frost, B. Partial Melting of Sulfide Ore Deposites During Medium and High-Grade Metamorphism. The Canadian Mineralogist. Vol. 40. 2002. pp. 1-18.

5. Andrew, G. Tomkins, B. Ronald, Frost & David R.M., Pattison. Arsenopyrite Melting During Metamorphism of Sulfide Deposits. The Canadian Mineralogist. Vol. 44 . 2006. pp. 1045 – 1062.

6. Yund, R. A. The System Ni-As-S: Phase Relations and Mineralogical Significance. American Journal of Science. Vol. 260. 1962. pp. 761-782.

7. Emelina, A. L., Alikhanian, A. S., Steblevskii, A. V. & Kolosov, E. N. Phase Diagram of the As-S system. Inorganic materials vol. 43, No. 2. 2007. pp. 95-104.

8. ACerS-NIST, Phase Equilibria Diagrams. CD-ROM Database, Version 3.2, NIST Standard Refence Database 31. National Institute of Standards and Technology (NIST). The American Ceramic Society. 2008.

9. Skinner, Brian J., Luce, Frederck D. & Makovicky, Emil. Studies of the Sulfosalts of Copper III. Phase and Phase Relations in the System Cu-Sb-S. Economic Geology. Vol. 67. 1972. pp. 924-938.

10. Ekman, A., Liukkonen, S & Sundholm, G. Fysikaalisen kemian taulukoita. 1977. 102 p.

11. Okamoto, H. Phase diagrams for binary alloys: desk handbook. ASM International. 2000. 714 P.

12. Cook, Nigel J., Ciobanu, Cristiana L., Wagner, T., Stanley & Christopher J. Minerals of the System Bi-Te-Se-S Related to the Tetradymite Archetype: Review of Classification and Compositional Variations. The Canadian Mineralogist. Vol. 45 . 2007. pp. 665-708.

13. Lin, J. C., Sharma, R. C. and Chang, Y. A. The Bi-S (Bismuth-Sulfur) system. Journal of Phase Equilibria. Vol. 17, No. 2. 1996. pp. 132-139.

14. Chang, Y.A, Neumann, J.P. & Choudary, U. V. Phase Diagrams and Thermodynamic Properties of Ternary Copper-Sulfur-Metal Systems. Incra Monograph VII, The Metallugy of Copper.1979. 191 p.

15. Standard Thermodynamic Properties of Chemical Substances. CRC PRESS LLC. 2000. Online accessed: May 2010. URL address: http://physics-of-molecules.odessit.org/library/db/thermodata_2400.pdf

16. Lange, W. und Schlegel, H. Die Zustandsbilder der Systeme Eisen – Antimon – Schwefel und Kobalt – Antimon – Schwefel. Z Metall, 42. 1951. pp. 257 – 268.

17. Alloy Phase Diagrams, Binary Alloy Phase Diagrams. ASM. Vol. 3. 1992. p. 104.

18. Lynch, D. C. Standard Free Energy of Formation of NiAsS. Metallurgical Transactions B, Vol. 13B. 1982. pp. 285-288.

19. Bryzgalov, I. A., Krivitskaya, N. N. and Spiridonov, E. M. First Finding of Nisbite and Aurostibite in the Eastern Transbaikal Region. Doklady Earth Sciences. Vol. 417, No. 8. 2007. pp. 1265–1267.

20. Bayliss, P. Isomorphous Substitution in Synthetic Cobaltite and Ullmannite. The American Mineralogist. Vol. 54. 1969. pp. 426-430.

21. Ullmannite. Mineral Data Publishing, version 1. 2005. Online accessed: May 2010. URL address: http://www.handbookofmineralogy.org/pdfs/ullmannite.pdf.

22. Raghavan, V. As-Cu-Fe-S (Arsenic-Copper-Iron-Sulfur). 2004. Phase Diagram Evaluations: Section II.

23. Müller, A. & Blachnik, R. Reactivity in the system copper–arsenic–sulfur I. The formation of Cu_3AsS_4, enargite. Thermochimica Acta 387.2002. pp. 153–171.

24. Gainov, R.R., Dooglav A.V., Pen'kov, I.N. Evidence for low-temperature internal dynamics in $Cu_{12}As_4S_{13}$ according to copper NQR and nuclear relaxation. Solid State Communications 140. 2006. pp. 544–548.

25. Müller, A. & Blachnik, R. Reactivity in the System Copper/Arsenic/Sulfur II. The Formation of CuAsS, (Lautite). Z. Anorg. Allg. Chem., 629. 2003. pp. 1833 – 1838.

26. Müller,A. Reaktivität im System Kupfer-Arsen-Schwefel und in den Entsprechenden Randsydtemen. Ph.D. These. Universität Osnabruck, Fachbereich Biologie/Chemie. 2000. 182 P.

27. Karup-Moller, S. & Makovicky, E. Skinnerite, Cu_3SbS_3, A New Sulfosalt From the llimaussaq Alkaline Intrusion, South Greenland. American Mineralogisl, Vol. 59.1974. pp. 889-895.

28. Craig, James R. & Lees, William R. Thermochemical Data for Sulfosalt Ore Minerals: Formation from Simple Sulfides. Economic Geology. Vol. 67, No.3. 1972. pp. 373 - 377.

29. Robert, R. Seal II, Eric J. Essene & William, C. Kelly. Tetrahedrite and Tennantite: Evaluation of Thermodynamic Data and Phase Equilibria. Canadian Mineralogist, vol. 28. 1990. pp. 725- 738.

30. Mookherjee, A. and Mishra, B. 'Derived' and Observed Sulphosalt-Sulphide Phase Assemblages Compared- A Case Study from Rajpura-Dariba. Mineralium Deposita 19. 1984. pp. 112 - 117.

31. Bryndzia, L. Taras. & Kleppa, O. J. High-Temperature Reaction Calorimetry of Solid and Liquid Phases in Part of the Quasi-Binary System Cu_2S-Sb_2S_3. America Mineralogy. Vol. 73. 1988. pp. 707 – 713.

32. Cambi, L. & Elli, M. Processi Idrotermali, Sintesi di Solfosali da Ossidi di Metalli e Metalloidi, Nota II – Cuprosolfoantimoniti. La Chimica E L'Industria. Vol. 47 – N. 2. 1965. pp. 136- 147.

33. Springer, G. Compositional Variations in Enargite and Luzonite. Mineral Deposita (Berl.) 4.1969. pp. 72-74.

34. Martinez Frias, J. Sulphide and Sulphosalt Mineralogy and Paragensis from the Sierra Almagrera Veins, Betic Cordillera (Se Spain). Estudios geol., 47. 1991. pp. 271-279.

35. Tatsuka, K. and Morimoto, N. Tetrahedrite Stability Relations in the Cu-Fe-Sb-S System. American Mineralogist. Vo. 62. 1977. pp. 1101-1109.

36. Bryndzia, L. Taras and Kleppa, O. J. Standard molar enthalpies of formation of sulfosalts in the Ag-As-S system and thermochemistry of the sulfosalts of Ag with As, Sb, and Bi. American Mineralogist. Vol. 74. 1989. pp. 243-249.

37. Sack, Richard O. Internally consistent database for sulfides and sulfosalts in the system Ag_2S–Cu_2S–ZnS–Sb_2S_3–As_2S_3. Geochimica et Cosmochimica Acta. Vol. 64, No. 22. 2000. pp. 3803–3812.

38. Wang, N. The Cu-Bi-S System: Results from Low Temperature Experiments. Institute of Mineralogy and Petrography. Mineralogical Magazine. vol. 58. 1994, pp. 201-204.

39. Agaeva, R. M. and Aliev, O. M. Phase Diagrams of the Systems $CuBiS_2$–$LnBiS_3$(Ln = La, Nd). Inorganic Materials. Vol. 41, No. 9. 2005. pp. 920–922. Translated from: Neorganicheskie Materialy. Vol. 41. No. 9. 2005. pp. 1051–1053.

40. Daqing. Wu. Phase relations in the Systems Ag_2S-Cu_2S-PbS and Ag_2S-Cu_2S-Bi_2S_3 and Their Mineral Assemblages. Geochemistry. Vol. 6, No.3. 1987. pp. 216-224.

41. Morgan, S.W.K. Zinc and Its Alloys and Compounds. Ellis Horwood Series in industrial metals. ISBN 0-470-20213-0. 1985. 238p.

42. Olekseyuk, I. D. & Tovtin, N. A. Phase equilibria and glass formation in the Zn-As-S system. Russian Journal of Inorganic Chemistry, 32 (10). 1987. pp. 1490-1492.

43. Andrew, G. Tomkins, David R.M. Pattision and B. Ronald Frost. On the Initiation of Metamorphic Sulfide Anatexis.Journal of Petrology. 2006. 25 p.

44. Chutas, Nathan I., Kress, Vicictor C., Ghiorso, Mark S. and Ricichard, O. Sackck. A solution model for high-temperature PbS-$AgSbS_2$-$AgBiS_2$ galena. American Mineralogist. Vol. 93. 2008. pp. 1630–1640.

45. Rosenqvist, T. Themochemical data for Metallurgists. University of Trondheim, department of Metallurgy. 1975. 93 p.

Appendix A

The melting temperatures (at 1 bar) of natural minerals and mineral associations found in sulfide ore deposits [4, 5, 8, 10, 14, 23, 25, 26, 9, 31, 35, 43].

Mineral or association	Chemical Formula	T_m (^oC)	Ref.
Native bismuth	Bi	271	Liu & Bassett, 1986
Bismuthinite	Bi_2S_3	755	[14]
Tsumoite	$BiTe$	540	Elliot, 1965
Tellurobismuthite	Bi_2Te_3	585	Elliot, 1965
Maldonite	Au_2Bi	375	Okamoto & Massalski, 1986a
Sobolevskite	$PdBi$	620	Elliot, 1965
Froodite	$PdBi_2$	485	Elliot, 1965
Kotulskite	$Pd(Te,Bi)$	720	Medvedeva et al., 1961
Micheneritess	$(PdPt)BiTe$	489 – 501	Cabri et al., 1973
Merenskyite	$(PdPt)(BiTe)_2$	740	Medvedeva et al., 1961
Antimony	Sb	631	[8, 10]
Aurostibite	$AuSb_2$	460	Okamoto & Massalski, 1986b
Calaverite	$AuTe_2$	464	Okamoto & Massalski, 1986c
Pyrargyrite	Ag_3SbS_3	485	Bryndzia & Kleppa, 1988
Pyrargyrite + argentite	$Ag_3SbS_3 + Ag_2S$	465	Bryndzia & Kleppa, 1988
Stibnite	Sb_2S_3	556	e.g. Bryndzia & Davis, 1989
		546	[31]
Miargyrite	$AgSbS_2$	510	Bryndzia & Kleppa, 1988
Jamesonite	$Pb_4FeSb_6S_{14}$	545	Chang & Knowles, 1977
Zinkenite	$Pb_9Sb_{22}S_{42}$	546	Salanci, 1979
Jordanite	$Pb_{14}(As,Sb)_6S_{23}$	549	Roland, 1968
Covelite	CuS	507	[9]
Chalcostibite	$CuSbS_2$	552	Bryndzia & Davis, 1989
Chalcostibite	$CuSbS_2$	552	Bryndzia(1989) & Skinner (1971)
(chalcostibite + stibnite)	$CuSbS_2 + Sb_2S_3$	496	Bryndzia(1989) & Skinner (1971)
skinnerite	Cu_3SbS_3	610	Bryndzia(1989) & Skinner (1971)
		608	Skinner et al. 1972 [4]
Dyscrasite	Ag_3Sb	558	Hansen & Aderko, 1958
Robinsonite	$Pb_4Sb_6S_{13}$	583	Salanci, 1979
Skinnerite	Cu_3SbS_3	610	Bryndzia & Davis, 1989
Miargyrite + stibnite	$AgSbS_2 + Sb_2S_3$	450	Bryndzia & Kleppa, 1988
Chalcostibite + stibnite	$CuSbS_2 + Sb_2S_3$	496	Bryndzia & Davis, 1989
Pyrrhotite	$Fe_{1-x}S$	1195	Freidrich, 1907
Pyrite + stibnite	$FeS_2 + Sb_2S_3$	494–545	Barton, 1971
Pyrrhotite + stibnite	$FeS + Sb_2S_3$	550	Barton, 1971
Stibnite + bismuthinite	$Sb_2S_3 + Bi_2S_3$	556–764	Solid solution at high T; Springer& Laflamme, 1971
Fe-tetrahedrite	$Cu_{9.96}Fe_2Sb_4S_{13}$	661	[35]
Fe-tetrahedrite	$Cu_{10.46}Fe_{1.5}Sb_{4.01}S_{13}$	643	[35]
Fe- tetrahedrite	$Cu_{11}FeSb_4S_{13}$	618	[35]
Tetrahedrite	$Cu_{11.58}Fe_{0.5}Sb_{4.02}S_{13}$	594	[35]
Tetrahedrite	$Cu_{12.30}Sb_{4.05}S_{13}$	573	[35]

Appendix A: continued

Mineral or association	Chemical Formula	T_m (^oC)	Ref.
Arsenic	As	814 (@36 atm.), 615(sublimation)	LENNTECH (water treatment solutions)
Sartorite	$PbAs_2S_4$	305	Kutolglu, 1969
	As_2S_4	310	Massalski et al. (1990)
Orpiment	As_2S_3	310	Hansen & Aderko, 1958
Realgar	AsS	321	Hansen & Aderko, 1958
Baumhauerite	$Pb_3As_4S_9$	458	Kutolglu, 1969
Arsenopyrite	FeAsS	670	Clark, 1960
Arsenopyrite + pyrite	$FeAsS + FeS_2$	491	Barton, 1969
Orpiment + loranditess	$As_2S_3 + Tl(Sb,As)S_2$	<275	Sobott, 1984
Lorandite + stibnite	$TlAsS_2 + (Sb,As)_2S_3$	<275	Sobott, 1984
Orpiment + galena	$As_2S_3 + PbS$ (44% As_2S_3)	300	Kutolglu, 1969
Orpiment + stibnite	$As_2S_3 + Sb_2S_3$	<310	Tomkins et al., 2004
Orpiment + bismuthinite	$As_2S_3 + Bi_2S_3$ (<30% As_2S_3)	<310	Based on Tm of As2S3, see also Walia & Chang, 1973 [43]
Tennantite	$Cu_{12}As_4S_{13}$	665	Bryndzia(1989) & Skinner (1971)
Tennantite	Cu_3AsS_3	640	Wernick & Benson (1957) [23]
		656	Kurz, Blachnik & Less (1989) [23]
		637	Zhumashev (1992) [23]
		670	Kuzgibekova, Sivak, Isabaev & Kompleksn (1993) [23]
Tennantite	$Cu_{12.31}As_4S_{13}$	665	Maske & Skinner (1971) [23]
Enargite	Cu_3AsS_4	665	Wernick & Benson (1957) [23]
		689	Cambi & Elli (1967), sealed in ampoule [23]
Enargite	Cu_3AsS_4= L Cu_3AsS_4= $Cu_{12+x}As_{4+y}S_{13}$ + L	672 672	Maske & Skinner (1971) [23] Cambi & Elli (1967), open crudble [23]
Enargite	Cu_3AsS_4= $Cu_{12+x}As_{4+y}S_{13}$ + L	642	Kurz (1984) [23]
Lautite	CuAsS ⇋ $Cu_{12+x}As_{4+y}S_{13}$ + As + L	574	[26]
Lautite	CuAsS ⇋ As + L	596	[26]
Cinnabar	HgS	825	Osadchii, 1990
Sphalerite	ZnS	1680	Freidrich, 1907
Galena	PbS	1114	Freidrich, 1907
Galena + argentite	$PbS + Ag_2S$	605	Urazov & Sokolova, 1983
Pyrite + galena	$FeS_2 + PbS$	719	Brett & Kullerud, 1967
Pyrrhotite + galena	$Fe_{1-x}S + PbS$	880	Freidrich, 1907
Po + Gn + Sph	FeSstoic. + PbS + ZnS	800	Mavrogenes et al., 2001
Py + Gn + Cpy + Sph	$FeS_2 + PbS + CuFeS_2 + ZnS$	730 @ 2 kbar	Stevens et al., 2005
Sphalerite + galena	ZnS + PbS	1040	Freidrich, 1907
Zinc	Zn	419(T_m), 927(B.P)	[41]

Appendix A: continued

Mineral or association	Chemical Formula	T_m (^oC)	Ref.
Pyrrhotite + sphalerite	$Fe_{1-x}S + ZnS$	1180	Freidrich, 1907
Pyrite + molybdenite	$FeS_2 + MoS_2$	735	Grover et al., 1975
Chalcocite	Cu_2S	1131	[14]
	Cu_2S	1127	[31]
Chalcopyrite	$CuFeS_2$	850	Craig & Kullerud, 1967
Bn + ISS	$Cu_5FeS_4 + CuFeS_2$	<800	Tsujimura & Kitakaze, 2004
Bn + Po	$Cu_5FeS_4 + FeS$	<800	Tsujimura & Kitakaze, 2004
Calaverite + altaite	$AuTe_2 + PbTe$	425	Prince et al., 1990
Native bismuth + gold	Bi + Au	241	Okamoto & Massalski, 1986a
Gold + calaverite	$Au + AuTe_2$	447	Okamoto & Massalski, 1986c
Petzite + electrum	$AuAg_3Te_2 + AuAgss$	<335	Cabri, 1965

Appendix B

Phase relations in the Ni-Sb-S system (compositions are in at. %) and the reaction schemes in the regions Ni-NiS-Sb and NiS-Sb_2S_3-Sb [16].

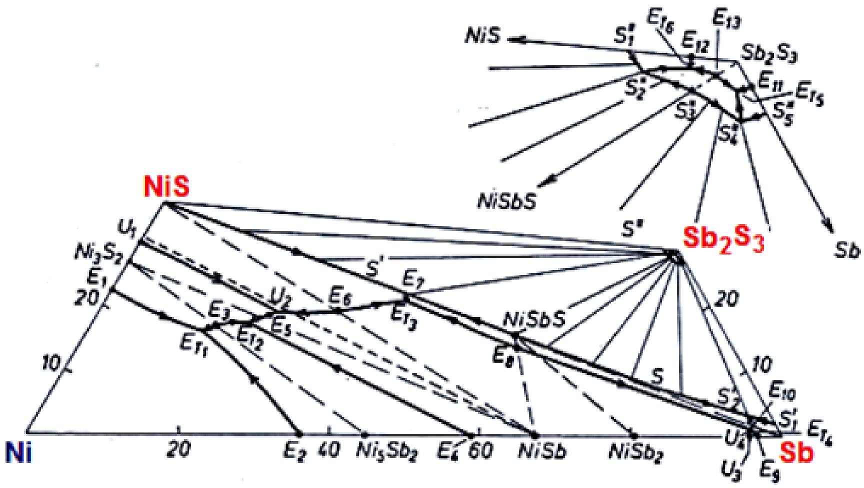

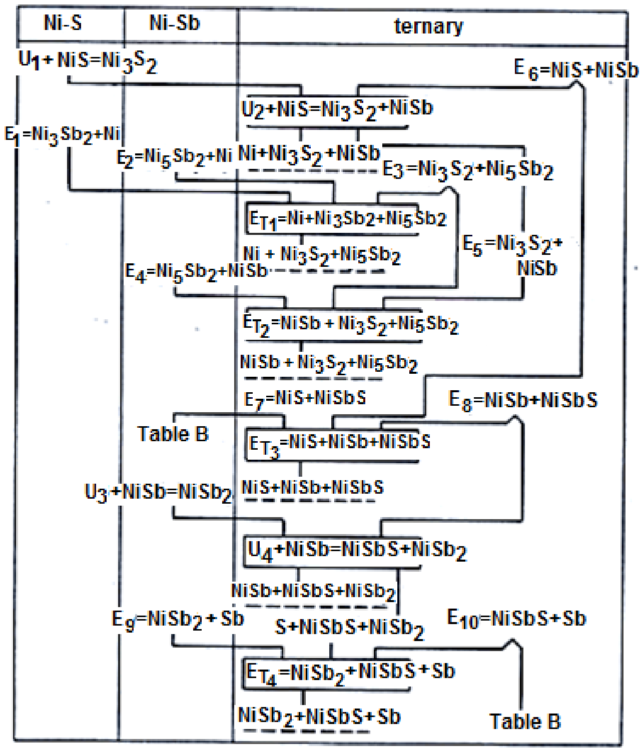

Table A: Reaction scheme of the region Ni - NiS - Sb

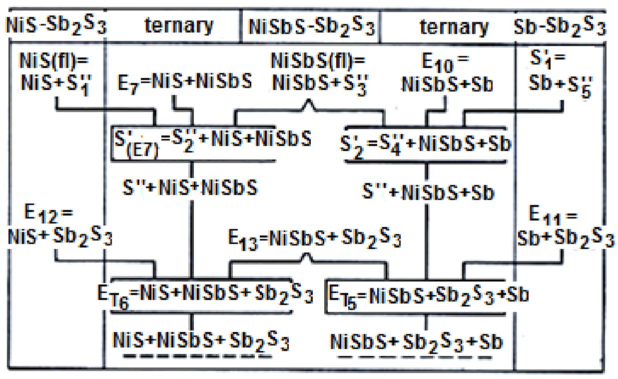

Table B: Reaction scheme of the region NiS - Sb_2S_3 - Sb

Appendix C

Standard state thermodynamic properties of selected sulfides and sulfosalts [44].

<table>
<tr><th>Mineral</th><th>Formula</th><th>$\Delta H^{\circ}_{f,298}$ (kJ/mol)</th><th>$\Delta S^{\circ}_{f,298}$ [J/(mol·K)]</th><th>$C^{\circ}_{Pf,298}$ [J/(mol·K)]</th><th>Molar volume (cm³)</th><th>Space group</th></tr>
<tr><td>Acanthite
(low-*T* structure)</td><td>Ag_2S</td><td>−31.21 (±0.71)*
-31.59†</td><td>143.5†</td><td>76.11†</td><td>34.23‡</td><td>*P*21/*n* (Z = 4)</td></tr>
<tr><td>Aramayoite</td><td>$Ag_3Sb_2BiS_6$</td><td>−94.3§</td><td>155.7§
151.9||</td><td>182.3#</td><td>54.14**</td><td>$P\bar{1}$ (Z = 2)</td></tr>
<tr><td>Argentite
(high-*T* structure)</td><td>Ag_2S</td><td>−32.6††</td><td>144.0††</td><td>76.5††</td><td>34.78††</td><td>*Im*3*m* (Z = 2)</td></tr>
<tr><td>Bismuthinite</td><td>Bi_2S_3</td><td>−135.2 (±2.4)*
-201.7†
−143.1††</td><td>200.4†††</td><td>122.2†††</td><td>75.50‡
75.520 (± 0.043)††</td><td>*Pbnm* (Z = 4)</td></tr>
<tr><td>Diaphorite</td><td>$Ag_3Pb_2Sb_3S_8$</td><td>−102.1§</td><td>126.8§
617.1||</td><td>391.6#</td><td>222.91#</td><td>*P*2₁/*c* (Z = 4)</td></tr>
<tr><td>Freieslebenite</td><td>$AgPbSbS_3$</td><td>−102.9§</td><td>117.1§
234.3||</td><td>148.1#</td><td>84.6§
86.07‡‡</td><td>*P*2₁/*a* (Z = 4)</td></tr>
<tr><td>Galena</td><td>PbS</td><td>−98.3††
−100.4††</td><td>91.2†††</td><td>49.5†††</td><td>31.492 ± 0.008††</td><td>*Fm*3*m* (Z = 4)</td></tr>
<tr><td>α-Matildite
(high-*T* structure)</td><td>$AgBiS_2$</td><td>−71.21 (±2.1)‡
−71.2§</td><td>181.1§||</td><td>105.6#</td><td>54.19‡</td><td>*Fm*3*m* (Z = 16)</td></tr>
<tr><td>β → α transition
(matildite)</td><td>195 °C‡</td><td>10.5 (±4.6)‡</td><td>22.5 (±9.8)‡</td><td>-</td><td>−0.31‡</td><td>-</td></tr>
<tr><td>β-Matildite
(low-*T* structure)</td><td>$AgBiS_2$</td><td>−81.71 (±6.7)‡
−82.8§</td><td>156.9§
158.6||</td><td>99.1#</td><td>54.40‡</td><td>*P*−3*m1* (Z = 3)</td></tr>
<tr><td>α-Miargyrite
(high-*T* structure)</td><td>$AgSbS_2$</td><td>−4.9207†
−75.6 (±3.2)‡</td><td>6.066†
170.0§</td><td>106.9#</td><td>55.93‡</td><td>*Fm*3*m* (Z = 16)</td></tr>
<tr><td>β → α transition
(miargyrite)</td><td>380 °C‡</td><td>8.7 (±1.4)§§‡</td><td>13.3 (±2.1)*‡</td><td>-</td><td>−1.53‡</td><td>-</td></tr>
<tr><td>β-Miargyrite
(low-*T* structure)</td><td>$AgSbS_2$</td><td>−4.1 (±2.3)‡
−12.4483||||
−84.6 (±4.6)‡</td><td>−5.459||||
157.4§</td><td>99.5#</td><td>55.93‡
55.50##</td><td>*C*2/*c* (Z = 8)</td></tr>
<tr><td>Stibnite</td><td>Sb_2S_3</td><td>−129.72 (± 3.75) ‡‡
−205†</td><td>182†</td><td>119.8†</td><td>73.37‡
73.406 (± 0.042)††</td><td>*Pbnm* (Z = 4)</td></tr>
</table>

Notes: P = 1 bar, T = 298.15 K. Transitions are from low- to high-temperature structures.
* From Bryndzia and Kleppa (1988b).
† From Mills (1974).
‡ From Bryndzia and Kleppa (1989).
§ Values used in binary models for this study.
|| Calculated (after Latimer 1952).
Calculated (after Wood and Fraser 1976).
** Mullen and Nowacki (1974).
†† From CRC Handbook of Chemistry and Physics (1994).
‡‡ Ito and Nowacki (1974).
§§ From Bryndzia and Kleppa (1988a).
|||| From Sack (2000).
Smith et al. (1997).

Standard enthalpies of formation of some sulfides from the stable modification of the elements [45].

Phase	ΔH^{o}_{298k} (kJ/mol.)
As_2S_3 (S)	-125.60 ± 12.56
As_2S_5 (S)	-146.54 ± 12.56
Sb_2S_3 (S)	-169.57 ± 21
NiS(S)	-92.95 ± 5.9
NiS_2(S)	-142.35 ± 16.75
Ni_2S_3(S)	-198.87 ± 10.47
CuS (S)	-50.66 ± 2.1
Cu_2S (S)	-82.06 ± 1.68
ZnS (S)	-201.8 ± 8.37

Appendix D

Non-variant reaction in the system Cu-As-S [26]; the abbreviations refer to points in Figure 17 (liquidus projection) of chapter 3.

Reaction	Temperature (°C)	Reaction type
L $\rightleftarrows$ ($Cu_{3-x}As$(HT)) + ($Cu_{2-x}S$)	800	eutektisch, e_4
L $\rightleftarrows$ ($Cu_{2-x}S$) + (As)	714	eutektisch, e_6
L + ($Cu_{3-x}As$(HT)) $\rightleftarrows$ ($Cu_{5-\delta}As_2$(HT)) + ($Cu_{2-x}S$)	708 ?	halb eutektisch, U_1
L_1' $\rightleftarrows$ L_1'' + (As) + ($Cu_{2-x}S$)	700 ?	ternär monotektisch, E_1
L $\rightleftarrows$ ($Cu_{3-x}As$(HT)) + (Cu) + ($Cu_{2-x}S$)	680 ?	ternär eutektisch, E_2
L $\rightleftarrows$ Cu_3AsS_4	672	kongruent, k_4
L $\rightleftarrows$ $Cu_{12+x}As_{4+y}S_{13}$	656	kongruent, k_5
L $\rightleftarrows$ Cu_3AsS_4 + ($Cu_{2-x}S$)	655 ?	eutektisch, e_8
L $\rightleftarrows$ Cu_3AsS_4 + $Cu_{12+x}As_{4+y}S_{13}$	655 ?	eutektisch, e_9
L $\rightleftarrows$ ($Cu_{2-x}S$) + $Cu_{12+x}As_{4+y}S_{13}$	650	eutektisch, e_{10}
L $\rightleftarrows$ $Cu_{12+x}As_{4+y}S_{13}$ + ($Cu_{2-x}S$) + Cu_3AsS_4	645 ?	ternär eutektisch, E_3
L $\rightleftarrows$ ($Cu_{5-\delta}As_2$(HT)) + (As) + ($Cu_{2-x}S$)	599 ?	ternär eutektisch, E_4
L + ($Cu_{2-x}S$) $\rightleftarrows$ $Cu_{12+x}As_{4+y}S_{13}$ + (As)	598	halb eutektisch, U_2
L + $Cu_{12+x}As_{4+y}S_{13}$ $\rightleftarrows$ $Cu_4As_2S_5$	597	peritektisch, p_2
L + $Cu_{12+x}As_{4+y}S_{13}$ + (As) $\rightleftarrows$ CuAsS	574	ternär peritektisch, P_1
L + $Cu_{12+x}As_{4+y}S_{13}$ $\rightleftarrows$ Cu_3AsS_4 + $Cu_4As_2S_5$	573	halb eutektisch, U_3
(As) + $Cu_{12+x}As_{4+y}S_{13}$ $\rightleftarrows$ ($Cu_{2-x}S$) + CuAsS	571	halb eutektoid, U_4
L_5' $\rightleftarrows$ L_5'' + Cu_3AsS_4 + ($Cu_{2-x}S$)	550 ?	ternär monotektisch, E_5
L + $Cu_4As_2S_5$ $\rightleftarrows$ $Cu_6As_4S_9$	530	peritektisch, p_3
L + ($Cu_{2-x}S$) $\rightleftarrows$ (CuS) + Cu_3AsS_4	507 ?	halb eutektisch, U_5
($Cu_{2-x}S$) + ($Cu_{3-x}As$(HT)) $\rightleftarrows$ (β-Cu_2S)	498	peritektoid, p_5
L + $Cu_{12+x}As_{4+y}S_{13}$ $\rightleftarrows$ $Cu_4As_2S_5$ + CuAsS	474	halb eutektisch, U_6
L + $Cu_4As_2S_5$ $\rightleftarrows$ $Cu_6As_4S_9$ + CuAsS	470 ?	halb eutektisch, U_7
L + $Cu_4As_2S_5$ $\rightleftarrows$ Cu_3AsS_4 + $Cu_6As_4S_9$	456	halb eutektisch, U_8
L $\rightleftarrows$ CuAsS + (β-As_4S_4)	316 ?	eutektisch, e_{12}
L $\rightleftarrows$ (As_2S_3) + $Cu_6As_4S_9$	309	eutektisch, e_{13}
L + $Cu_6As_4S_9$ $\rightleftarrows$ Cu_3AsS_4 + (As_2S_3)	306 ?	halb eutektisch, U_9
L + CuAsS $\rightleftarrows$ $Cu_6As_4S_9$ + (β-As_4S_4)	280 ?	halb eutektisch, U_{10}
L $\rightleftarrows$ $Cu_6As_4S_9$ + (β-As_4S_4) + (As_2S_3)	270 ?	ternär eutektisch, E_6
L $\rightleftarrows$ (As) + (α-As_4S_4) + CuAsS	195 ?	ternär eutektisch, E_7
L + Cu_3AsS_4 $\rightleftarrows$ (As_2S_3) + (CuS)	180 ?	halb eutektisch, U_{11}
L $\rightleftarrows$ (β-S_8) + (CuS) + (As_2S_3)	114 ?	ternär eutektisch, E_8

Appendix E

Standard free energies of formation and vaporization; standard state is $S_2(g)$ at unit fugacity (even though this cannot exist below 900°C) [45].

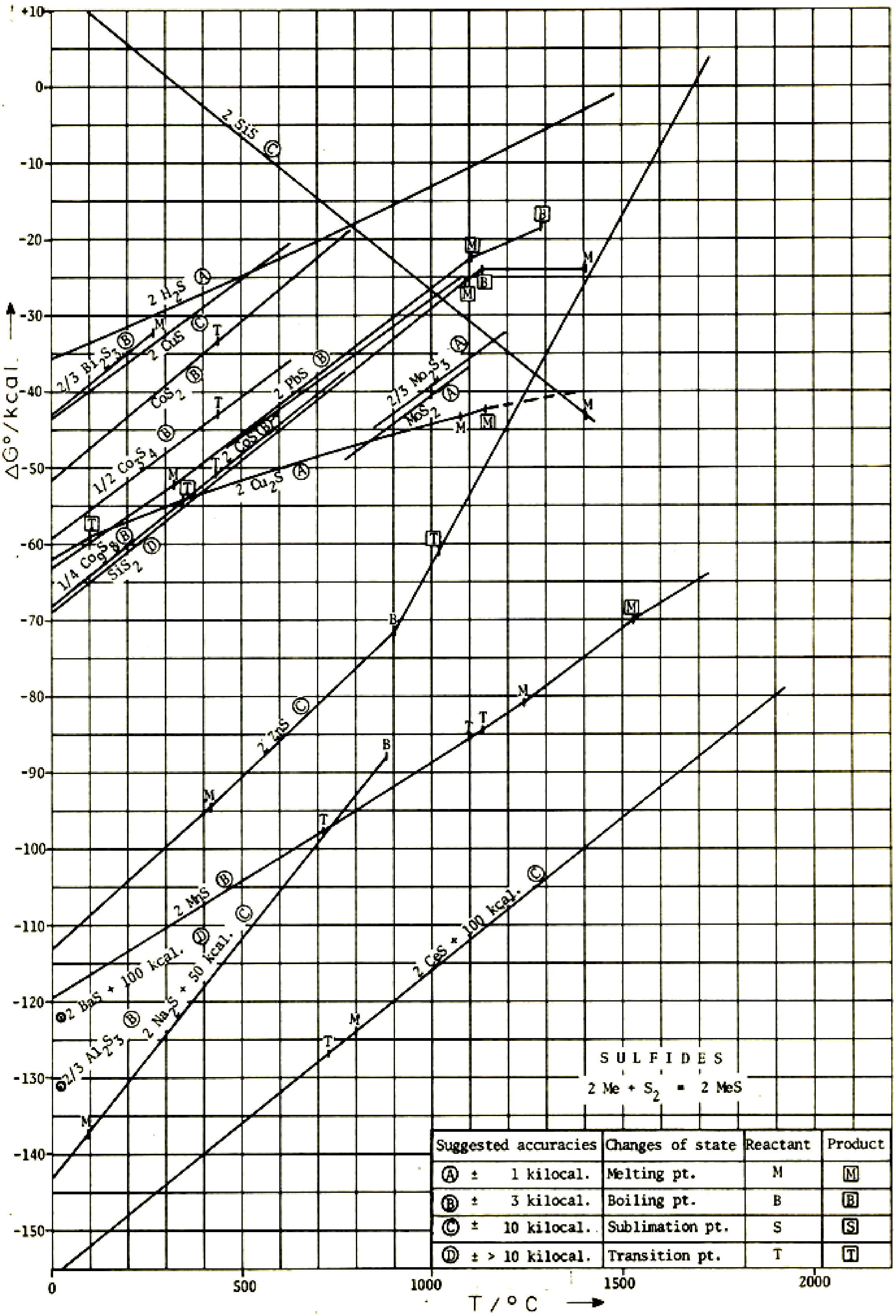

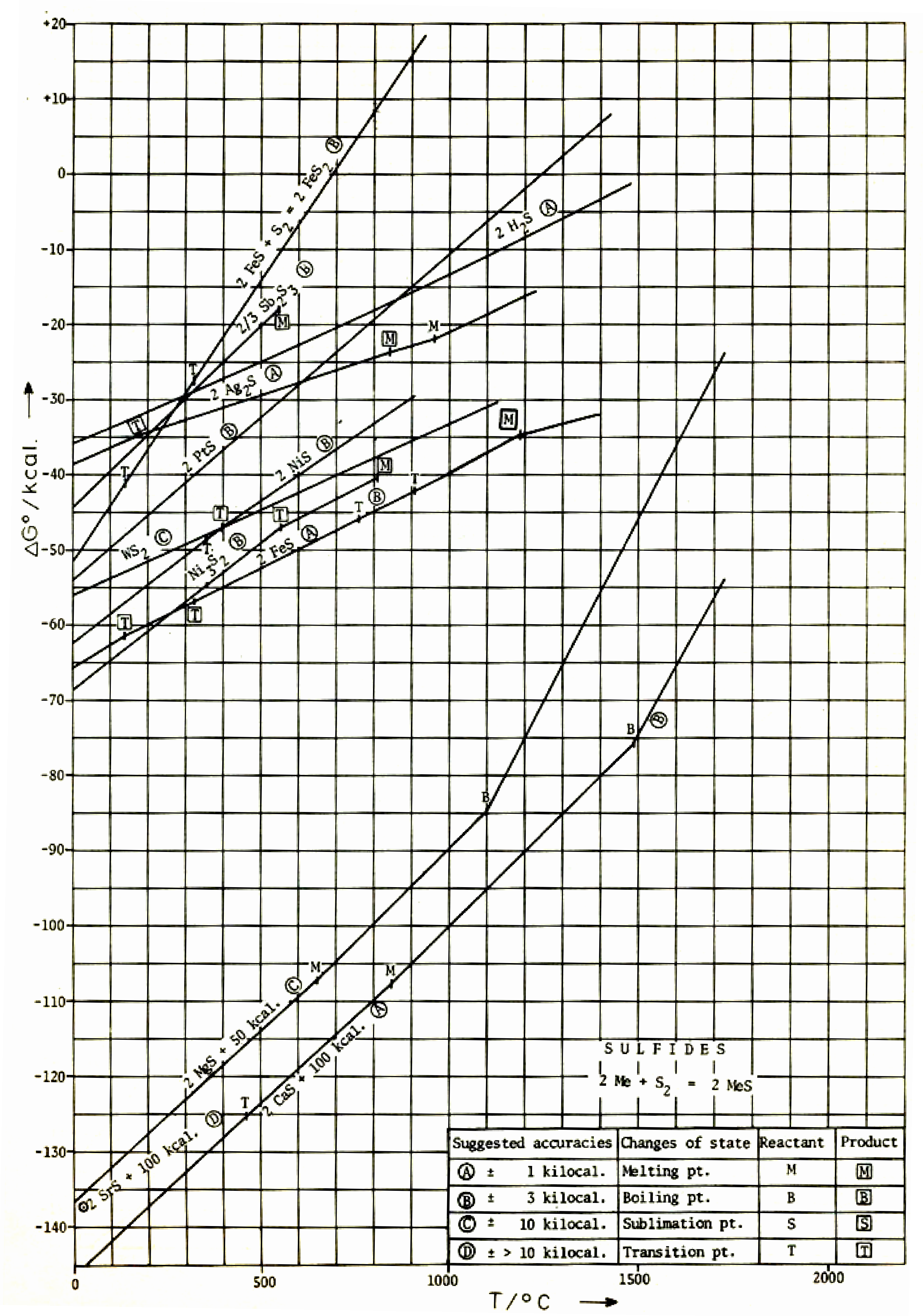
SULFIDES
2 Me + S2 = 2 MeS
ΔG° / kcal.
T / °C
2 FeS + S2 = 2 FeS2 Ⓑ
2 H2S Ⓐ
2/3 Sb2S3 Ⓑ
2 Ag2S Ⓐ
2 PtS Ⓑ
2 NiS Ⓑ
WS2 Ⓒ
Ni3S2 Ⓑ
2 FeS Ⓐ
2 MgS + 50 kcal. Ⓒ
2 CaS + 100 kcal. Ⓐ
2 SrS + 100 kcal. Ⓓ
Suggested accuracies
Ⓐ ± 1 kilocal.
Ⓑ ± 3 kilocal.
Ⓒ ± 10 kilocal.
Ⓓ ± > 10 kilocal.
Changes of state
Melting pt.
Boiling pt.
Sublimation pt.
Transition pt.
Reactant
M
B
S
T
Product
M
B
S
T

HELSINKI UNIVERSITY OF TECHNOLOGY PUBLICATIONS IN MATERIALS SCIENCE AND ENGINEERING

TKK-MT-202	Miettinen, J., Tentative thermodynamic description of ternary Fe-Mo-B, Fe-Nb-B, Fe-Ti-B and Fe-V-B systems. 2008
TKK-MT-203	Kekkonen, M. (ed.), Materials production and synthesis / 2008
TKK-MT-204	Heikinheimo, E., Selin, L. (editors), Defect Structure and Reactivity of Solids. 2009
TKK-MT-205	Miettinen, J., Thermodynamic description of the Fe-Nb-Ti-V-C-N system. 2009
TKK-MT-206	Miettinen, J., Kytönen, H., Thermodynamic descriptions of Fe-Mn-Si, Fe-Mn-B and Fe-Si-B systems. 2009
TKK-MT-207	Huitu, K., Kekkonen, M., Holappa, L., Novel Steelmaking Processes. 2009
TKK-MT-208	Bunjaku, A., Holappa, L., Thermodynamic properties of NICKEL laterite ores. 2009
TKK-MT-209	Heikinheimo, E., Selin, L. (editors), Quantitative electron probe microanalysis in materials science. Graduate School Seminar, September 25, 2009 at TKK, Espoo, Finland
TKK-MT-210	Keski-Honkola A., Vaajoki, A., Oksanen, J., Hämäläinen, M., Ag-Bi-Cu-Sn seoksen termodynaaminen mallintaminen FactSage-ohjelmalla. 2009
TKK-MT-211	Kekkonen, M., (ed.), Materials Production and Synthesis / 2009 MT-0.3201
TKK-MT-212	Isomäki, I., Hämäläinen, M., Pirso, J., Ferreira, J., Braga, H. Thermodynamic and Structural Study of Quaternary Ni-rich Fe-Ni-Ti-W Phase Diagram. 2009
TKK-MT-213	Heikinheimo, E., (ed.), Activity Report 2007 – 2009. Department of Materials Science and Engineering. 2010
TKK-MT-214	Tesfaye Firdu, F., Taskinen, P., Sulfide Mineralogy – Literature Review. 2010
TKK-MT-215	Tesfaye Firdu, F., Taskinen, P., Densities of Molten and Solid Alloys of (Fe, Cu, Ni, Co) – S at Elevated Temperatures – Literature Review and Analysis. 2010

ISBN 978 952-60-3273-3
ISSN 1455-2329